UNIVERSITY OF CALIFORNIA

Los Angeles

The Glioblastoma Perivascular Microenvironment

A dissertation submitted in partial satisfaction of the requirements for the degree of

Doctor of Philosophy in Molecular Biology

By

Yasmin Ghochani

2016

ABSTRACT OF THE DISSERTATION

The Glioblastoma Perivascular Microenvironment

By

Yasmin Ghochani

Doctor of Philosophy in Molecular Biology

University of California, Los Angeles, 2016

Professor Harley Kornblum, Chair

Glioblastoma (GBM) is the most fatal and aggressive brain tumor in adults, and with an average prognosis of 15 months, new therapeutic avenues are desperately needed. A major contributing factor to GBM malignancy is the maintenance of a GBM stem cell (GBMSC) population within a tumor propagating perivascular microenvironment, though the specific interactions mediating vascular support of GBMSCs are not well understood. We thus developed a comprehensive interactome, outlining all putative vascular endothelial cell (ECs) ligand-GBMSC receptor interactions as identified through whole transcriptome profiling of ECs and GBMSCs isolated from the same freshly resected primary patient GBM samples. We revealed a prominent role for the perivascular niche (PVN) interactions to be in promoting tumor cell migration and invasion. From our interactome, the function of the EC-secreted Integrin Binding Sialoprotein (IBSP) angiocrine in promoting Proneural GBMSC migration, proliferation,

and a transition to a more aggressive Mesenchymal phenotype was specifically demonstrated. Our analyses are a first to report on such a detailed interrogation of the mechanisms of GBMSC dependence on the PVN, and provide a large database to fuel further research in this area. The supplementary files accompanying this dissertation include Spreadsheet 1 with the complete overall GBMSC vs. glial progenitor cell (GPC) differential expression analysis (DEA) (a), and the associated Ingenuity Pathway Analysis (IPA) Diseases and Functions $p<0.05$ (b); Spreadsheet 2 with the complete overall GBM-EC vs. EC DEA (a), the significantly enriched IPA Canonical Pathways, $p<0.05$ (b), and the IPA-predicted Upstream Regulators, $p<0.05$ (c); Spreadsheet 3 with the GBM-EC extracellular factors DEA (a), and GBM-SC plasma membrane (PM) proteins DEA (b); Spreadsheet 4 with the GBM-EC extracellular factors FPKM expression units (a), GBMSC PM proteins FPKM expression units (b), and our comprehensive PVN interactome by FPKM expression units (c), where $FPKM>4$ are highlighted in red; and Spreadsheet 5 with the complete overall IBSP vs. Control DEA, $FDR<0.001$ (a), the significantly enriched IPA Canonical Pathways, $p<0.05$ (b), the IPA-predicted Upstream Regulators, $p<0.05$ (c), and associated IPA Diseases and Functions, $p<1.5e-6$ (d).

The dissertation of Yasmin Ghochani is approved.

Luisa M. Iruela-Arispe

Bennett G. Novitch

Stanley Thomas Carmichael

Linda M. Liau

Harley I. Kornblum, Committee Chair

University of California, Los Angeles

2016

Dedication

This work is dedicated to Alister Hosseini, my exceptionally brilliant, unconditionally loving, and unimaginably supportive husband

and to my courageous mother, Balgis Hadjianpoor, whose determination continues to inspire and empower me.

Table of Contents

List of Figures and Tables……..…….vii

Acknowledgements…….....x

Biographical Sketch…….....xiii

Chapter 1. Introduction……..……..1

Chapter 2. A novel glioblastoma cell perivascular niche interactome reveals a prominent role for the IBSP angiocrine in tumor propagation……12

Abstract……12

Introduction…….……...13

Results……..…….……..15

Discussion……..…….……....68

Experimental Procedures……..……75

Chapter 3. Summary and Perspectives……..……..…....88

References……..92

Figures and Tables

Chapter 2

Table 1. Summary table of patient sample characteristics……..18

Figure 1. Approach, cell-type verification, and samples……..20

Table 2. Diseases and Functions significantly associated with GMBSC differential expression as compared to non-neoplastic GPCs……22

Figure 2. Gene expression profile of all 39 samples sequenced……23

Table 3. Canonical Pathways enriched in GBM-EC differentially regulated genes..…..27

Figure 3. Select predicted to be activated Upstream Regulators of GBM-EC differentially regulated genes……..28

Table 4. PVN interactome according to DEA……...33

Table 5. Known PVN ligands and their putative interactions with GBMSCs within the comprehensive intractome according to FPKM expression units……..……34

Figure 4. Select putative interaction groups within the comprehensive intractome…….35

Table 6. Diseases and Functions significantly associated with all angiocrines and their putative GBMSC PM interaction partners from the comprehensive interactome…….37

Table 7. SIBLING upregulation and FPKM expression units in GBM-ECs……..…40

Chapter 2 (continued)

Figure 5. IBSP GBM-EC expression confirmation and correlation with poor patient survival……41

Figure 6. Endogenous and exogenous IBSP effect on gliomasphere cultures……45

Figure 7. The IBSP peptide promoted HK217 migration in hydrogel-based microenvironment……...48

Figure 8. HK301 gliomaspheres verified the migration-inducing properties of IBSP…..50

Figure 9. An HT method to assess cellular dispersion in hydrogel microenvironments……53

Figure 10. An shRNA screen of GBMSC receptors revealed ITGs mediating IBSP action on GBMSC migratory capacity……54

Figure 11. ITGαV antibody blockers abrogated IBSP migratory action on gliomaspheres……56

Figure 12. IBSP promoted PN gliomasphere proliferation……..……58

Figure 13. IBSP expression correlates with reduced patient survival in only PN GBMs……59

Figure 14. Overlapping canonical pathways significantly enriched by IBSP treatment as predicted by IPA……63

Chapter 2 (continued)

Figure 15. Multiple known Mesenchymal pathway regulators were also significantly activated upstream regulators of the IBSP-induced set of dysregulated genes……..64

Figure 16. IBSP promoted a Mesenchymal expression signature…….65

Figure 17. IBSP pre-treatment induced lasting tumor promoting functional changes…67

Acknowledgements

I would like to thank Dr. Harley Kornblum, upon whose scientific and creative guidance and support this research has come to fruition. It was a great privilege to complete my dissertation with his patient collaboration in providing me the space and freedom to explore and appreciate scientific research as I did, yet interjecting with invaluable advice and direction when needed. The support and guidance of my thesis committee members, Dr. Luisa Iruela-Arispe, Dr. Ben Novitch, Dr. Tom Carmichael, and Dr. Linda Liau, were also paramount in completing this work, and I am grateful for their gracious participation in my training. I would also like to thank all the members of the Kornblum lab for their kindness, wisdom, and friendship.

I must express my deepest gratitude to my mother, Balgis Hadjianpoor, whose encouragement and courage have inspired me throughout this and every journey I've undertaken, and my sister, Mariam Ghochani, whose intelligence, wisdom and kindness continue to impress, influence, and humble me.

The following collaborators have contributed greatly to this work, and I'm grateful to them for all their help, time, and for believing in my scientific vision for this project.

Jack Mottahedeh: Processing freshly resected brain tissue for cell type isolation

Giovanni Coppola: Bioinformatics and intellectual contribution to scientific direction

Riki Kawaguchi: Data analysis of RNA-seq study

Fuying Gao: Data analysis of microarrays

Stephanie Seidlits: 3D Hydrogel migration assays, and intellectual contribution to scientific direction

Alireza Sohrabi: 3D Hydrogel migration assays

University of CA, Los Angeles (UCLA) Johnson Comprehensive Cancer Center (JCCC):

Iris Williams: Fluorescence-activated cell sorting

Andre Gregorian: Gliomasphere cultures

Anjelica Cardenas: Gliomasphere cultures

UCLA Molecular Screening Shared Resource (MSSR):

Robert Damoiseaux: Targeted shRNA screen

Bryan France: Assisted in targeted shRNA screen

UCLA Brain Tumor Translational Resource (BTTR):

William Yong: Pathology on tumors and distributing GBM samples

Greg Lucey: Brain tumor sections and immunohistochemistry

Bowen Wei: Brain tumor sections and immunohistochemistry

Moe Ishihara: Immunohistochemistry

UCLA Neuroscience Genomics Core:

Joseph DeYoung: RNA amplification and cDNA library preparation

UCLA Broads Stem Cell Research Center:

Suhua Feng: RNA sequencing

UCLA Pathology & Laboratory Medicine:

Clinical Cytogenetics Core:

Nagesh Rao: Cytogenetics analyses

Clinical Microarray Core:

Xinmin Li: Microarrays

Linda M Liau: Surgical resection of tumors

Gary W Mathen: Surgical resection of non-transformed tissue

Steve A Goldman: Intellectual contribution to scientific direction

S Thomas Carmichael: Intellectual contribution to scientific direction

Harley I Kornblum: Guidance, insight, and supervision of all studies

Chapter 2 is a version of a work in preparation for publication:

A novel glioblastoma cell perivascular niche interactome reveals a prominent role for the IBSP angiocrine in tumor propagation. Ghochani Y, Kawaguchi R, Sohrabi A, Mottahedeh J, Goldman SA, Carmichael ST, Seidlits SK, Coppola G, Kornblum HI.

This work was partially funded by the UCLA Neural Repair training grant, and the UCLA Tumor Cell Biology training grant.

Biographical Sketch

Yasmin Ghochani

Education:

Ph.D. Student. Molecular Biology Interdepartmental Program

University of California, Los Angeles, 2011-2016.

Dissertation: The Glioblastoma Perivascular Microenvironment

M.S. Biological Sciences with emphasis on neuroendocrinology and molecular biology of reproduction

University of California, San Diego, 2007-2009.

Thesis: Hormonal Interactions in Progesterone Regulation of Gonadotropin Gene Expression.

B.S. Double Major: Biochemistry and Cell biology, Cognitive Neuroscience

University of California, San Diego, 2003-2008.

Honors and Awards:

Tumor Cell Biology Training Program at UCLA - NIH T32 CA 009056. 2015-2016.

The Training Program in Neural Repair at UCLA - NIH T32 NS 744915. 2012-2013.

Honorable Mention: National Science Foundation (NSF), Graduate Research Fellowship Program. 2012.

UCSD Chancellor's Undergraduate Research Scholarship. 2007-2008.

UCSD Provost's Honor (11 undergraduate quarters). 2003-2008.

Publications:

Le Belle JE, Sperry J, Ngo A, **Ghochani Y**, Laks DR, López-Aranda M, Silva AJ, and Kornblum HI (2014). Maternal Inflammation Contributes to Brain Overgrowth and Autism-Associated Behaviors through Altered Redox Signaling in Stem and Progenitor Cells. *Stem Cell Reports*. 10.1016/j.stemcr.2014.09.004

Ghochani Y, Jasjit S, Mellon P, and Thackray V (2012). FoxL2 Is Required for Synergy between Activin and Progestins on the Follicle-Stimulating Hormone β-Subunit Promoter. *Endocrinology* 153(4):2023-33.

Lundius EG, Sanchez-Alavez M, **Ghochani Y**, Klaus J, and Tabarean IV (2010). Histamine Influences Body Temperature by Acting at H1and H3 Receptors on Distinct Populations of Preoptic Neurons. *J. Neurosci.* 30: 4369-4381.

Thackray V, Hunnicutt J, Memon A, **Ghochani Y**, and Mellon P (2009). Progesterone Inhibits Basal and Gonadotropin-Releasing Hormone Induction of Luteinizing Hormone β-Subunit Gene Expression. *Endocrinology* 150(5): 2395-2403.

Employment:

2010-2011 Biology Professional. Inflammation Research Program. Allergan Inc. Irvine, CA.

2009 Research Assistant. Molecular and Integrative Neurosciences Department (MIND). The Scripps Research Institute. La Jolla, CA.

2007-2008 Undergraduate Researcher. Cognitive Neuroscience Laboratory. University of CA, San Diego. La Jolla, CA.

2006-2008 Laboratory/Research Student Assistant. Structural and Computational Biology and Design. Pfizer Global Research and Development. San Diego, CA.

2006 Summer Research Intern. Cell Biology. The Scripps Research Institute. La Jolla, CA.

2005-2006 Laboratory Assistant. FFA Sciences. San Diego, CA

Teaching Assistant

University of CA, Los Angeles. Los Angeles CA.

Life Sciences Introduction to Molecular Biology (LS2-3), Spring2015

Life Sciences Laboratory (LS23L) , Spring2014

University of CA, San Diego. La Jolla, CA.

Mammalian Physiology (BIPN 100), Fall2006, Spring2009, Summer2009

Neurobiology of Cognition, Winter2009

Biochemical Techniques Laboratory (BIBC 103), Fall2008

Endocrinology (BICD 140), Winter2008

Chapter 1

Introduction

Glioblastoma

Every year, approximately 200,000 new cases of glioma are diagnosed across the globe, thus constituting the most common type of brain tumor in adults (Parkin et al., 2005). These tumors are more common in men than women, display an increased incidence with age, and constitute 29% of all primary tumors of the central nervous system (CNS) (Dolecek et al., 2012). Risk factors, other than age, include having a family history of glioma, and high exposure to ionizing radiation and environmental carcinogens (Bondy et al., 2008; Fisher et al., 2007; Omuro and DeAngelis, 2013).

Gliomas are categorized into 4 groups based on histopathological characteristics that demonstrate the level of malignancy, according to guidelines set forth by the World Health Organization (WHO) (Louis et al., 2007). By far the most common, and deadly of these tumors are the grade IV Glioblastomas (abbreviated GBM as they were previously termed Glioblastoma multiforme), with an annual incidence of 5.26/100000 people (Omuro and DeAngelis, 2013), and an average survival of 15 months (Stupp et al., 2009). In total, GBMs constitute 54% of all gliomas, and 82% of all cases of malignant glioma, or the Grade III and IV tumors together (Dolecek et al., 2012; Omuro and DeAngelis, 2013). The Grade III tumors are anaplastic variants of astrocytoma, oligodendroglioma, and oligoastrocytoma (or mixed glioma), named so according to immunophenotypical resemblances to putative glial cells of origin. Grade I and II, or low

grade gliomas are diffuse tumors that are more differentiated and thus less malignant, though they too can have fatal outcomes as they progress and/or recur as a higher grade glioma (i.e. secondary tumors).

With increasing malignancy more aggressive phenotypic changes occur that include anaplasia or a loss of cellular structure and/or orientation, or de-differentiation, increased cellularity and mitotic activity, necrosis, and extensive neovascularization that leads to the formation of a leaky network of vasculature that is reflected as enhancement on the MRI of GBM tumors (Louis et al., 2007), and is considered a pathological hallmark of these tumors (Brem et al., 1972). Another phenotypic characteristic of GBMs is their highly invasive nature, and though they do not metastasize to the outside of CNS, they do infiltrate the brain parenchyma, thus preventing the complete surgical resection of the tumor.

Treatment

The currently available GBM therapeutic options are very limited, and do not provide for a substantial advantage in patient survival. Following surgical resection of the tumor, a combination of radio- and chemotherapy is administered as the current standard of care (Stupp et al., 2005). Temozolomide (TMZ), a DNA alkylating agent, is the most commonly used chemotherapeutic agent in treating GBMs, though it has been shown to be most effective in presence of the O6-methylguanine-DNA methyltransferase (MGMT) promoter hypermethylation (Hegi et al., 2005). The MGMT gene is a DNA repair enzyme, which is epigenetically silenced in approximately 40% of

GBMs (Wick et al., 2014). The remaining 60% of the patients with MGMT overexpression are thus inherently resistant to DNA alkylating agents. With the current standard combination therapy, patients experience a survival benefit of 3 months (12 vs. 15 months), signifying the urgent need for new avenues of therapy for GBM patients.

GBM tumor heterogeneity

GBMs are a considerably heterogeneous group of tumors, and harbor a wide array of chromosomal and epigenetic abnormalities (e.g. 1p/19q deletion, isocitrate dehydrogenase 1 (IDH1) mutation, epidermal growth factor receptor (EGFR) amplification, copy number variations of chromosomes 7 and 10, and MGMT promoter hypermethylation), which may be assessed in biopsy or resected samples for their diagnostic and prognostic significance (van den Bent et al., 2010; van den Bent et al., 2009; van den Bent et al., 2003; Yan et al., 2009). For example, a GBM that has the IDH1 mutation, R132H, has a more favorable prognosis than most other GBMs (Noushmehr et al., 2010; Verhaak et al., 2010), although virtually all patients succumb to their disease.

The GBM tumor heterogeneity also extends to the tumor's molecular expression profiles. The most comprehensive genome-wide expression analysis of a large cohort GBM samples, by The Cancer Genome Atlas (TCGA), has defined 4 tumor subclasses termed Classical, Mesenchymal (Mes), Proneural (PN), and Neural, according to the differential expression of the most variable genes (Verhaak et al., 2010). This classification scheme not only provides significant insight into the various oncogenic

and functional pathways that promote tumor propagation, but has also been correlated to various genetic aberrations. Classical GBMs often have EGFR amplification and the EGFR vIII rearrangement, chromosomes 7 and 10 copy number aberrations, CDKN2A loss, and Notch and Sonic hedgehog pathway activations. Mesenchymal tumors typically have loss of NF1, along with upregulation TNF-α and NF_KB pathway genes. The Proneural subtype is characterized by PDGFRA and Olig2 activations, or point mutations in the IDH1 and TP53 genes. Furthermore, Proneural GBMs' expression profile resemble that of lower grade gliomas and secondary GBMs, and Neural samples exhibit upregulation of neuronal markers.

Recently, a modified version The TCGA classification (see Chapter 2, Experimental Procedures) was developed by our lab to extend the classification scheme to GBM-derived primary human cell lines (Laks et al., 2016). Most notably, the Neural subclass was eliminated in our classification model, as it is thought to represent normal brain tissue. This is evident in the fact that normal brain tissue samples classified as Neural in the original TCGA classification scheme (Verhaak et al., 2010), and when normal brain cells were removed from GBM samples, no neural classification of the remaining tumor cells was obtained (Patel et al., 2014).

Through the various refinements of the classification scheme (Cooper et al., 2010; Huse et al., 2011; Laks et al., 2016; Phillips et al., 2006; Verhaak et al., 2010), however, the PN and Mes classifications have persisted as functionally meaningful subclasses, with the Mes tumors displaying elevated aggressiveness and worse prognosis than the PN tumors (Colman et al., 2010; Pelloski et al., 2005; Phillips et al., 2006). This may in part be due to the classification of the IDH1 mutant GBMs almost

exclusively to the PN group, though, not all PN GBMs have the IDH1 mutation (Verhaak et al., 2010). Interestingly, PN glioblastomas have been shown to recur as Mes tumors (Phillips et al., 2006), and all subclasses have been shown to co-exist within a single tumor sample (Patel et al., 2014), indicating a dynamic transcriptional landscape for the heterogeneous GBM cell population to allow for maximal tumor propagating properties, where a more aggressive expression and phenotypic character may be adopted by GBM cells as the tumor progresses.

GBMSCs

GBMs contain a small fraction of cells that display stem cell-like properties, though the defining features of this population are debated, and are evolving through the increasing body of research (Reviewed in (Lathia et al., 2015; Schonberg et al., 2014)). However, there is general consensus that this proposed GBM stem cell/stem cell-like cell population (GBMSC) hold, exclusively, the tumor initiating properties that allow them to form tumors in orthotopic xenotransplatation models, thus recapitulating the growth of a tumor in possession of the parent tumor's cellular heterogeneity.

GBMSCs share a number of features with brain stem and progenitor cells. They have been modeled in an *in vitro* culture system, virtually identical to that used in culturing neural stem cell (NSCs) (Reynolds et al., 1992; Reynolds and Weiss, 1992), that enriches for stem cell properties, such as self-renewal and proliferation over multiple passages (Hemmati et al., 2003; Ignatova et al., 2002; Singh et al., 2003). This culture system requires the addition of growth factors, epidermal growth factor (EGF),

basic fibroblast growth factor (bFGF), in a serum-free condition that allows for non-adherent spheroid culturing of NSC (neurospheres), or GBMs (gliomaspheres). GBM-derived primary gliomasphere cultures are enriched for cells that display multipotency in terms of giving rise to a heterogenous mixture of cells that are representative of the original tumor in *in vivo* xenotransplantation (Galli et al., 2004; Hemmati et al., 2003; Nunes et al., 2003; Rich and Eyler, 2008; Singh et al., 2004), and are currently the most accepted in vitro model of GBMs (Laks et al., 2016).

Despite the aggressive research efforts to identify a universal marker to distinguish and/or isolate GBMSCs from GBM tumor resections, and *in vitro* gliomasphere cultures, GBMSCs have demonstrated great antigenic heterogeneity, and multiple tumor initiating phenotypes have been investigated and reported in literature (Nishide et al., 2009; Schonberg et al., 2013; Singh et al., 2004). Indeed, this may be representative of the variety of stem and progenitor cells that have been shown to have the capacity to give rise to gliomas (Alcantara Llaguno et al., 2009; Jackson et al., 2006), including neural stem cells, and various glial progenitors, though the topic of the GBM cell of origin remains a hotly debated issue (reviewed in (Stiles and Rowitch, 2008; Zong et al., 2012). Nevertheless, the putative NSC marker CD133 (Prominin-1) was first shown by Singh et al. to be expressed by GBM tumor initiating cells (Singh et al., 2004), and remains the most commonly used GBMSC marker. Other reported GMBSC markers include A2B5, CD44, CD15 (SSEA1), L1CAM, integrin α6, and a number of NCS markers including Musashi, Nestin, Nanog, Oct4, Sox2 (Schonberg et al., 2014), which may be representative of the various GBM subclasses and

heterogeneity, or due to tumor adaptive responses to take the phenotype of the normal structures they occupy (Cuddapah et al., 2014).

However, the most abundant cycling cell population in the adult human brain are glial progenitor cells (GPCs) (Nishiyama et al., 2009; Sim et al., 2009). GPC expression of A2B5 antibody recognized gangliosides (Nunes et al., 2003), NG2/CSPG4, and platelet-derived growth factor-α receptor (Nishiyama et al., 2009; Sim et al., 2011) are up-regulated in gliomas (Ogden et al., 2008; Shih and Holland, 2006), and GPCs have been shown to give rise to genomically and histologically human-like GBMs in various mouse models (Assanah et al., 2006; Liu et al., 2011). Furthermore, in functional assays of self-renewal and tumor initiation, A2B5 expressing cells isolated from a number of patient derived GBM cell lines enrich for SC properties and contain the majority of tumor initiating (including CD133 expressing) cells in most tumors (Auvergne et al., 2013; Ogden et al., 2008; Tchoghandjian et al., 2010). In light of their high expression in the majority of GBMs, their capacity to give rise to tumors, representative of the heterogeneity of the parent tumor, in orthotopic xenotransplatation models at low density, and their demonstrated potential to give rise to high grade gliomas in various animal models, A2B5-expressing cells were chosen in our studies as a most informative and inclusive GBMSC population of cells.

The Glioblastoma perivascular microenvironment

The glioblastoma tumor microenvironment is most significantly characterized in terms of a perivascular niche composed of hyperproliferative and hyperpermeable

neovasculture that support the tumor cells, especially GBMSCs, which actively seek out the vessels (Montana and Sontheimer, 2011), migrate along them, halting intermittently in their path to divide and proliferate (Farin et al., 2006; Watkins et al., 2014), and are maintained in close association with the vascular endothelial cells (ECs) (Calabrese et al., 2007). The GBM PVN is thought to be similar to the NSC perivascular niches that promotes NSC proliferation and survival (Louissaint et al., 2002; Palmer et al., 2000b; Ramirez-Castillejo et al., 2006; Shen et al., 2004), and in fact, in most other non-neoplastic tissues, stem cells are maintained within similar protective niches (Fuchs et al., 2004; Moore and Lemischka, 2006). Furthermore, in the normal brain dividing and newly-born neuroblasts migrating along the rostral migratory stream (RMS) are also supported by blood vessels scaffolds (Bozoyan et al., 2012; Saghatelyan, 2009).

The GBM vascular network also contributes to vasogenic edema and tissue hypoxia, thus facilitating further tumor angiogenesis and a selection for a more malignant tumor phenotype. Their contribution to hypoxia and hemorrhage is attributed to dead vessel ends and loss of vascular hierarchy (Jain et al., 2007b). The perivascular microenvironment is composed not only of GBMSCs and the vasculature, but also of a number other non-tumor cells, including infiltrating microglia, astrocytes, and pericytes, among others, which further contribute to the aberrant structure, and the complex network of signaling of a tumor propagating niche. The PVN infiltrating immune cells, for example, are thought to be a driving force behind induction of inflammatory angiogenesis when localized to the peri-necrotic tissue, and contributors to tumor cell proliferation and migration, mainly through cytokine signaling pathways (Lewis and Pollard, 2006; Watters et al., 2005). Furthermore, astrocyte endfeet, which are an

essential component of the blood brain barrier (BBB), cover approximately 99% of vessel surfaces in a healthy brain (Iadecola and Nedergaard, 2007; Mathiisen et al., 2010). Glioma cells xenotransplated into rodent brains, however, have been shown to disrupt the astrocytic endfeet and degrade the perivascular basement membrane as they move along the vessels and invade into the surrounding parenchyma. (Farin et al., 2006; Watkins et al., 2014; Zagzag et al., 2000), and in doing so perhaps contributing to the leakiness of the GBM associated vasculature.

In light of the major contribution of the PVN to GBMSC behavior, it is of great importance to dissect and investigate the specific PVN interactions and signaling pathways, in order to identify viable therapeutic targets for intercepting mechanisms that specifically promote GBMSC maintenance and invasion. The vessels themselves are at the core of the PVN-GBMSC interactions and multiple efforts have been made to identify a core set of dysregulated genes in the anomalous tumor vasculature, though the main focus of much research has been on the tumor regulation of angiogenesis. Most notably, Dietrich et al. used laser microdissection of vessels and microarray gene expression profiling of flash-frozen samples to identify 95 differentially expressed genes, including upregulation of angiopoietin 2 (ANGPT2), endothelial cell specific molecule 1 (ESM1), CD93, EGF, latrophilin and seven transmembrane domain containing protein1 (ELTD1) and Filamin A interacting protein 1-like (FILIP1L) in GBM vasculature as compared to normal vessels, which revealed glioma VEGFA- and TGFβ2-mediated regulation of the ECs (Dieterich et al., 2012). GBM-ECs, of course, overexpress VEGF receptors, whose activation promote angiogenesis and increase vascular permeability (Jain et al., 2007a).

Unfortunately, the anti-angiogenic therapeutic, bevacizumab, which targeted VEGF-mediated angiogenesis, was proven to not be efficacious, as it either failed to induce a response, or led to tumor resistance. This may be due to other signaling pathways through which GBMSCs may regulate ECs, and promote angiogenesis such as basic fibroblast growth factor (bFGF), Tie-2, stromal-cell derived factor-1α (SDF-1α), and/or it may be a result of tumor cells' increase in invasiveness, aggressiveness, and effectively their loss of dependence on the PVN blood vessels (Jhaveri et al., 2014). Though there have been such extensive research efforts into tumor mediated regulation of angiogenesis, there has been much less investigation into the EC-mediated regulation of GBMSC tumor propagating mechanisms.

It was demonstrated by Calabrese et al. that GBM-EC secreted factors promote brain tumor SC self-renewal and proliferation *in vitro*, and tumor initiation and growth in xenotransplatation models (Calabrese et al., 2007). Thus, there exists an obvious need to understand the spatial, and temporal dependence of these cells, as an adaptive and dynamically heterogeneous population, on the vasculature in order to determine how they can be intercepted. Among the few pathways that have been reported in vascular regulation of GBMSCs, GBM Notch signaling activation through 1. endothelial ligands Delta-like 4 (DLL4) and Jagged-1 leading to increased GBMSC proliferation and tumor angiogenesis (Zhu et al., 2011), and 2. endothelial Nitric Oxide leading to increased gliomasphere formation, and again tumor angiogenesis in an autocrine manner (Charles et al.; Jeon et al., 2014), are of notable significance, as they validate GBM-EC regulation of GBMSCs tumor propagating signaling pathways. However, the complexity and a comprehensive view of such interactions have not been previously explored and

are of paramount importance in uncovering novel niche-dependent pathways that specifically promote GBMSC aggressiveness and invasion. As GBMSCs are the significant contributors to therapeutic resistance and tumor recurrence (Bao et al., 2006a; Schonberg et al., 2014), the niche that promotes their stem-like properties may provide a novel and effective therapeutic avenue in treating GBMs.

Chapter 2

A novel glioblastoma cell perivascular niche interactome reveals a prominent role for the IBSP angiocrine in tumor propagation

Abstract

Glioblastoma stem cells (GBMSCs) proliferate and invade in a perivascular niche (PVN) due to their interactions with endothelial cell (EC) angiocrines, though the specific factors and signaling pathways responsible are largely unknown. Here, we generated an angiocrine driven interactome of the entire set of secreted or cell surface molecules expressed respectively in GBM-associated ECs and GBMSCs, from the same freshly resected primary tumor samples, to elucidate the interactions underlying GBMSC dependence on its perivascular niche. We demonstrated that a substantial role of the PVN interactions is in promoting GBMSC invasion. As such, we characterized the role of the Integrin Binding Sialoprotein (IBSP), and demonstrated its action in promoting gliomasphere migration, and proliferation, specifically in a Proneural subset of GBMs. We further revealed a novel role for this angiocrine in promoting a Mesenchymal (Mes) shift, which was accompanied by the upregulation of the Mes master transcriptional regulator, STAT3, and along with a predicted activation state of NF_KB pathway.

Introduction

Glioblastoma (GBM; WHO grade IV) is the most common and lethal brain tumor in adults (Louis et al., 2007; Wen and Kesari, 2008), with limited treatment option due to therapy resistance and recurrence (Kaisorn L. Chaichana et al., 2010; Omuro and DeAngelis, 2013). GBMs display great genotypic, transcriptomic, and phenotypic heterogeneity, and various molecular characterization efforts, most comprehensive of which by Verhaak et al. in the Cancer Genome Atlas (TCGA), have revealed at least three clinically relevant subtypes termed Classical, Mesenchymal (Mes), and Proneural (PN) (Phillips et al., 2006; Verhaak et al., 2010). The subtypes can co-exist within a single tumor, and may represent different stages of pathology and malignancy, evident in PN-Mes transitions associated with increased tumor aggressiveness (Bhat et al., 2013; Patel et al., 2014; Phillips et al., 2006; Piao et al., 2013). Self-renewing and multipotential GBM stem cell (GBMSC) populations have also demonstrated great heterogeneity (Nishide et al., 2009; Schonberg et al., 2013; Singh et al., 2004), perhaps representing the tumor initiating phenotypes of the various molecular subtypes (Huse et al., 2011). GBMSCs expressing the glial progenitor cell (GPC) ganglioside markers that are recognized by the A2B5 antibody have, however, been shown to contain the majority of such tumor initiating phenotypes in most GBMs and display tumor SC properties (Auvergne et al., 2013; Ogden et al., 2008; Shih and Holland, 2006; Tchoghandjian et al., 2010).

Contributing to clinical prognosis, GBMSCs promote and rely on an elaborate network of tumor associated vessels that form a structurally and functionally aberrant

microvascular environment (Jain et al., 2007b; Norden et al., 2009). A great deal of work has focused on the mechanisms by which tumor angiogenesis occurs. GBMSC-secreted pro-angiogenic factors, such as vascular endothelial growth factor (VEGF), allow for extensive neovascularization at various regions within the tumor microenvironment (Anderson et al., 2008; Miletic et al., 2009). However, there has been less investigation of GBM interactions with specific factors produced by vascular endothelial cells that support GBMSC tumor propagation, despite the abundant evidence that these cells survive, proliferate, and invade within a perivascular niche (Calabrese et al., 2007; Montana and Sontheimer, 2011), and contribute to chemo- and radiotherapy resistance due to such interactions (Bao et al., 2006b; Borovski et al., 2013; Schonberg et al., 2013). A portion of the tumor endothelial cells (ECs) and pericytes, are thought to be derived from neoplastic GBMSCs themselves, thus allowing for vascular support and tumor growth (Cheng et al., 2013; Ricci-Vitiani et al., 2010; Wang et al., 2010). Tethering to the vascular basement membrane by the interaction of extracellular matrix components such as laminins, and tumor cell integrin receptors (Lathia et al., 2010), GBMSCs disrupt the normal perivascular basement membrane as they migrate along the blood vessels (Farin et al., 2006; Watkins et al., 2014; Zagzag et al., 2000), thus invading the surrounding tissue, though knowledge of the specific invasion-promoting mediators of such interactions is limited. Here we have generated an angiocrine driven interactome of ECs with A2B5 expressing GBMSCs from fresh primary GBM patient samples to elucidate the factors and signaling pathways underlying GBMSC interactions within the perivascular niche and their role in promoting tumor propagation.

Results

Enrichment and isolation of perivascular niche endothelial cells and A2B5+ GBMSCs from freshly resected human brain tissue

We obtained fresh human brain samples from patients undergoing GBM tumor resection surgeries or brain surgeries for treatment of non-neoplastic conditions (non-transformed cortical resections) under an approved University of California, Los Angeles (UCLA) Institutional Review Board (IRB) protocol. Information on patient diagnoses and sample characteristics can be found in Table 1. Our non-transformed samples were collected from children and adolescents (3-19 years old) and consist of small sections of healthy cortex or white matter, which were resected to gain access to deeper epileptic or otherwise pathological brain structures, and were considered normal according to MRI, and electroencephalogram studies (Table 1A). Samples from which specific cell types were isolated, were collected either in the operating room (non-transformed) or immediately following surgery through pathology, which allowed for a limited time between tissue resection and our purification schemes (Figure 1A). We utilized magnetic activated cell sorting (MACS) against CD31 to enrich for ECs, followed by flow cytometry (fluorescent-activated cell sorting: FACS) to purify A2B5+ GBMSCs or GPCs from the EC-depleted samples. RNA extraction immediately followed cell type isolation, thus best representing the *in vivo* transcriptome of the cells, as acquired through RNA sequencing (RNA-seq). RNA-seq was also carried out on small pieces of un-dissociated parent GBMs and non-transformed grey matter (GM) and white matter (WM) as controls. To ensure that the A2B5+ cells isolated from GBM samples were indeed tumor

cells and not normal GPCs from non-neoplastic parenchyma, we carried out EGFR and PTEN Fluorescence in situ Hybridization (FISH) and compared the chromosomal abnormalities of the our purified cells to those of the clinical case through the UCLA Clinical Cytogenetics Core. In the tumor tested (Figure 1B) both GBMSCs and the clinical case had 100% EGFR amplification and were clearly concordant. For the PTEN cytogenetic status, however, only 24% of the isolated GBMSCs showed 10q deletion, as compared to the 60% reportedly detected in the original tumor. This difference is likely because deletions in formalin fixed paraffin embedded (FFPE) sections of the clinical case were overcalled due to truncation artifacts. Ingenuity Pathway Analysis (IPA, Quiagen) of the diseases and functions associated with the significantly differentially regulated genes of the GBMSCs as compared to the GPCs (differential expression analysis, DEA, $p<0.005$) revealed a significant enrichment of tumor pathways promoting proliferation, survival, and CNS neoplasia (Table 2. Complete overall GBMSC vs. GPC DEA (a), and diseases and functions $p<0.05$ (b), can be found in Spreadsheet 1), thus further confirming our purification of tumor cells in A2B5-targeted sorting of cells from GBM samples. Validating the EC enrichment protocol, a panel of EC specific markers were significantly upregulated (reported as $\log_2$ transformed fold change or logFC) in the EC transcriptome as compared to the whole GBM sample, from which they were isolated (Figure 1C; $p<0.005$). Principle-component analysis (PCA) was carried out to demonstrate the distribution of the overall expression profiles of the GBM tissue and cell samples used in this study. Also included in the PCA are GM, WM, and the ECs and GPCs collected from the same or similar non-transformed samples (Figure 1D). The PCA plot high-lighted the great variability in

GBMSC transcriptome, though this observation is in accordance to the well-recognized heterogeneity that exits among GBMs. A heatmap illustration of the transcriptome of all the samples compared to the GM and WM (and GM and WM compared to ECs, in order to visualize all samples and their unique transcriptomes) showed similarity of expression profiles of the samples within each cell/tissue type, and the readily distinguishable expression profiles of each type from each other (Figure 2). In total, we sequenced 10 GBM samples and their ECs, 8 of which were samples used in the study as they were primary GBM samples with no prior treatments, from 5 of which we isolated the GBMSC cellular fraction as well in order to generate a GBMSC-EC perivascular niche interactome (GBM sample used in the analyses are highlighted in Table 1-B).

A

Sample #	Cell Fraction Isolated for RNA-seq	Age	Gender	Surgical notes:
12	EC, GPC	19	M	Left hemispherectomy for Left MCA perinatal stroke
13	EC, GPC	13	M	Left temporal occipital craniotomy for cortical dysplasia
14	GM and WM, EC	5	F	Left frontal temporal craniotomy for resection of left cortical dysplasia.
15	GM and WM	12	F	Right hemispherectomy for diffuse right hemisphere cortical malformation and seizures with Lennox-Gastaut.
16	GM and WM	3	F	Right hemicraniotomy for epilepsy secondary to right intraventricular teratoma.

B

Sample #	Diagnosis	Cell Fraction Isolated for RNA-seq	Age	Gender	Characteristics and Cytogenetics
GBM1	GBM Recurrent/(prior Gliosarcoma/concurrent meningioma)	Unsorted, EC	48	M	Maximum Ki67: 75%; MGMT Not Methylated; Trisomy 7, Monosomy 10
GBM2	GBM, Primary Recurrent	Unsorted, EC	38	M	Maximum Ki67: 80%; MGMT Not Methylated; Monosomy 10 plus 10q loss
GBM3	Oligoastrocytoma, WHO grade III	Unsorted, EC	34	M	Maximum Ki67: 7%; MGMT Methylated; IDH1 positive; 1p/19q co-deletion
GBM4	GBM Primary with gigantocellular features	Unsorted, EC, GBMSC	66	M	Maximum Ki67: 90%; MGMT Not Methylated; Multiple copies 7, 1,19. Monosomy 19. 10q loss
GBM5	GBM, Primary with oligodendroglial component	Unsorted, EC	42	M	Maximum Ki67: 70%; MGMT Methylated; IDH1 positive; Monosomy 10
GBM6	GBM Primary	Unsorted, EC	77	F	Maximum Ki67: 40%; MGMT Methylated; EGFR amplified
GBM7	GBM Primary	Unsorted, EC, GBMSC	55	F	Maximum Ki67: 20%; MGMT Not Methylated; EGFR amplified; Monosomy 10
GBM8	GBM Primary	Unsorted, EC, GBMSC	36	M	Maximum Ki67: 40%; EGFR amplified; Monosomy 10
GBM9	GBM Primary	Unsorted, EC, GBMSC	59	M	Maximum Ki67: 40%; MGMT Not Methylated; EGFR amplified; EGFR vIII positive
GBM10	GBM Primary (outside report suggests gliosarcoma)	Unsorted, EC, GBMSC	58	M	Maximum Ki67: 70%; MGMT Not Methylated; Polysomy 1 and 19. 10q loss
GBM11	GBM Primary	Unsorted, EC	71	M	Maximum Ki67: 20%; MGMT Not Methylated; EGFR vIII positive; Monosomy 10

Table 1 Summary table of patient sample characteristics.

Patient diagnoses/surgical notes, age, and gender, along with GBM Ki67 index, MGMT methylation status, EGFRvIII, EGFR amplification, and cytogenetic abnormalities were obtained from patient pathology reports. The highlighted samples were used in our differential expression and total expression interactome analyses. (A) Non-transformed samples. (B) Tumor samples.

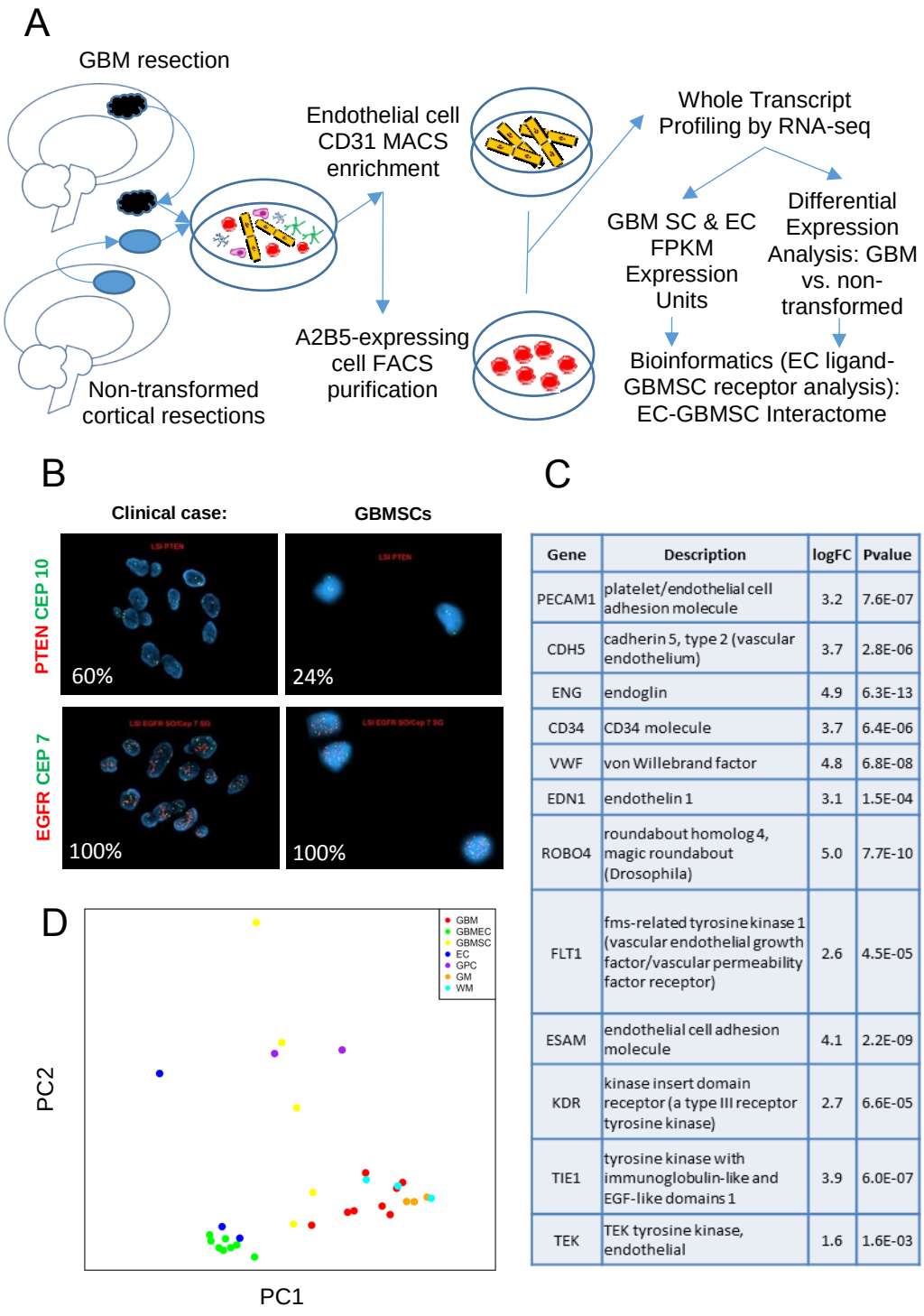

Gene	Description	logFC	Pvalue
PECAM1	platelet/endothelial cell adhesion molecule	3.2	7.6E-07
CDH5	cadherin 5, type 2 (vascular endothelium)	3.7	2.8E-06
ENG	endoglin	4.9	6.3E-13
CD34	CD34 molecule	3.7	6.4E-06
VWF	von Willebrand factor	4.8	6.8E-08
EDN1	endothelin 1	3.1	1.5E-04
ROBO4	roundabout homolog 4, magic roundabout (Drosophila)	5.0	7.7E-10
FLT1	fms-related tyrosine kinase 1 (vascular endothelial growth factor/vascular permeability factor receptor)	2.6	4.5E-05
ESAM	endothelial cell adhesion molecule	4.1	2.2E-09
KDR	kinase insert domain receptor (a type III receptor tyrosine kinase)	2.7	6.6E-05
TIE1	tyrosine kinase with immunoglobulin-like and EGF-like domains 1	3.9	6.0E-07
TEK	TEK tyrosine kinase, endothelial	1.6	1.6E-03

Figure 1 Approach, cell-type verification, and samples.

(A) Outline of the experimental approach for isolation, and whole transcriptome analysis of stem/progenitor and endothelial cells from GBM and non-neoplastic cortical and/or white matter resections, and the differential or total expression bioinformatics analyses of data in order to generate a GBM perivascular interactome. (B) Cytogenetic analysis of A2B5+ GBMSCs and their parent tumor (clinical case). Clinical case had 100% EGFR amplification and 60% 10q deletion, and GBMSCs had 100% EGFR amplification and 24% 10q deletion. (C) Endothelial markers upregulated in MACS-enriched GBM-ECs as compared to the whole un-dissociated parent tumor obtained through paired differential expression analysis ($p<0.005$). (D) PCA of un-dissociated primary GBM samples (red), and the GBMSCs (green) and GBM-ECs (yellow) derived from them, along with non-transformed GPCs (purple), ECs (blue), GM (orange), and WM (aqua) samples sequenced.

Categories	Diseases or Functions Annotation	p-Value	Predicted Activation State	Activation z-score	# Molecules
Cellular Growth and Proliferation	proliferation of cells	7.31E-05	Increased	4.187	581
Cell Death and Survival	cell survival	2.15E-03	Increased	2.909	223
Cancer, Organismal Injury and Abnormalities	growth of malignant tumor	6.28E-04	Increased	2.885	77
Cancer, Neurological Disease, Organismal Injury and Abnormalities	gliomatosis	6.48E-04	Increased	2.88	135
Cancer, Cellular Development, Cellular Growth and Proliferation, Organismal Injury and Abnormalities, Tumor Morphology	proliferation of tumor cells	4.56E-03	Increased	2.846	78
Cancer, Neurological Disease, Organismal Injury and Abnormalities	central nervous system tumor	1.68E-04	Increased	2.688	158
Cancer, Organismal Injury and Abnormalities	neuroepithelial tumor	4.58E-04	Increased	2.409	137
Cell Cycle, Cellular Assembly and Organization, DNA Replication, Recombination, and Repair	segregation of chromosomes	6.31E-05	Increased	2.359	28
Cell Death and Survival	apoptosis of vascular endothelial cells	3.87E-03	Increased	2.329	19
Cellular Assembly and Organization, DNA Replication, Recombination, and Repair	chromosomal congression of chromosomes	4.26E-05	Increased	2.236	7
Cell Cycle, DNA Replication, Recombination, and Repair	homologous recombination	4.44E-04	Increased	2.167	26

Table 2 Diseases and Functions significantly associated with GMBSC differential expression as compared to non-neoplastic GPCs.

Only significantly activated functions as predicted according to Z-score>2 are shown ($p<0.005$). The number of molecules used by IPA for this prediction is shown in the last column from left.

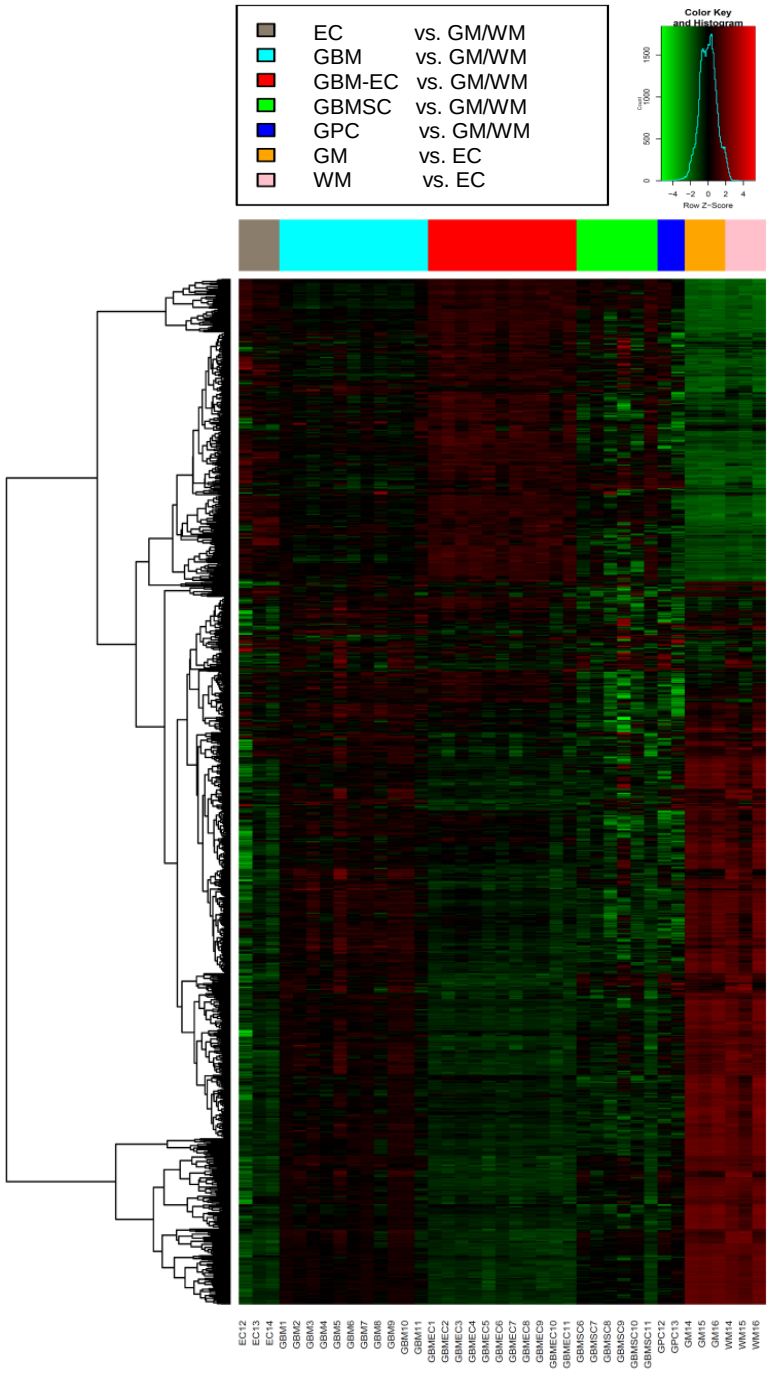

Figure 2 Gene expression profile of all 39 samples sequenced.

Genes significantly dysregulated (FDR<0.1) in each sample in comparison to the overall expression of GM and WM, and GW and WM as compared to the overall EC transcription profile are shown. The colored ribbon designates tissue/cell type associated with the area of the heatmap, where shown in gray are EC, aqua are undissociated GBM tissue sample, red are GBM-EC, green are GBMSC, blue are GPCs, orange are GW, and pink are WM samples' transcriptomes.

GBM-EC differential expression revealed known and novel putative pathways in regulation of the GBM microenvironment

To investigate the extensive bidirectional tumor promoting perivascular interactions facilitated by abnormal GBM microvascularization (Charles and Holland, 2010), multiple efforts have been made to identify a core set of dysregulated genes associated with the aberrant GBM vascular phenotype as compared to normal brain vessels. However, utilizing laser microdissection of vessels from cryopreserved samples and microarray expression profiling, have not revealed a comprehensive view of all the differentially expressed genes in tumor endothelial cells (Dieterich et al., 2012; Pen et al., 2007), due to a combination of technical limitations such as RNA quality, and expression profiling of not only endothelial cells but also vessel associated pericytes and potentially other contaminating cells such as GBMSCs that are closely associated with the vasculature. Our acute vascular endothelial cell enrichment technique from freshly resected samples combined with RNA-seq transcriptome profiling have allowed for the most extensive characterization of the changes in gene expression in GBM endothelial cells to date (Complete overall GBM-EC vs EC DEA (a), significantly enriched IPA Canonical Pathways $p<0.05$ (b), and IPA-predicted Upstream Regulators $p<0.05$ (c), are shown in Supplementary Spreadsheet 2). We identified 1150 differentially regulated GBM endothelial genes ($p < 0.005$) capturing known regulators of the GBM perivascular interactions such as ANGPT2 (Scholz et al., 2016; Stratmann et al., 1998), VEGF-A induced endothelial genes ESM1, NOX4, PXDN (Dieterich et al., 2012), and TGFβR1 (Krishnan et al., 2015), along with many novel putative targets

(Supplementary Spreadsheet 2a). Canonical pathway investigation of our targets revealed a prominent role in glioma invasiveness and HIF1α signaling (Table 3; Supplementary Spreadsheet 2b to view the genes used for these predictions). Examining the activated upstream regulators of GBM-EC dysregulated expression revealed not only the known EC regulators in GBM such as TGFβ, VEGF, HIF1α, and NOS2, (Dieterich et al., 2012; Jeon et al., 2014; Musumeci et al., 2015), but also novel putative regulators such as Estrogen Receptor signaling (ESR1, z-score=4.3, p-value=$2.3x10^{-5}$), and IL1A/B (IL1A: z-score=2.7, p-value=$1.6x10^{-5}$; IL1B: z-score=2.1, p-value=$7.8x10^{-7}$; Figure 3; Supplementary Spreadsheet 2c). IL1A and IL1B have been shown to promote inflammatory angiogenesis in other cancers (Murakami et al., 2013; Voronov et al., 2003), and may play a similar role in GBM endothelial regulation not only by GBMSCs, but also perhaps by the infiltrating inflammatory cells within the tumor microenvironment, as immune cell adhesion and diapedesis pathways were also significantly upregulated in the GBM endothelial cells. Thus our non-probe based transcriptome inquiry of the freshly resected GBM-ECs provides the opportunity for investigation of multiple dysregulated genes and pathways within the GBM perivascular niche that are under the influence of not only GBMSCs but also a network of other parenchymal and stromal cells. This may allow for a more accurate and complete examination of the GBM vascular abnormalization that contributes to tumor propagation.

Ingenuity Canonical Pathways	-log(p-value)	Ratio
EIF2 Signaling	6.54E00	1.41E-01
Granulocyte Adhesion and Diapedesis	5.27E00	1.3E-01
Inhibition of Matrix Metalloproteases	2.78E00	1.79E-01
Pyrimidine Deoxyribonucleotides De Novo Biosynthesis I	2.58E00	2.27E-01
Hepatic Fibrosis / Hepatic Stellate Cell Activation	2.39E00	9.29E-02
Atherosclerosis Signaling	2.39E00	1.05E-01
Airway Pathology in Chronic Obstructive Pulmonary Disease	2.36E00	3.75E-01
Agranulocyte Adhesion and Diapedesis	2.25E00	8.99E-02
Unfolded protein response	1.97E00	1.3E-01
Uracil Degradation II (Reductive)	1.94E00	5E-01
Heme Degradation	1.94E00	5E-01
Thymine Degradation	1.94E00	5E-01
Bladder Cancer Signaling	1.77E00	1.03E-01
Oncostatin M Signaling	1.75E00	1.47E-01
Creatine-phosphate Biosynthesis	1.73E00	4E-01
Nucleotide Excision Repair Pathway	1.7E00	1.43E-01
LXR/RXR Activation	1.67E00	9.09E-02
Oxidative Phosphorylation	1.58E00	9.17E-02
Glycerol Degradation I	1.56E00	3.33E-01
Regulation of eIF4 and p70S6K Signaling	1.47E00	8.22E-02
HIF1α Signaling	1.38E00	8.82E-02
Glioma Invasiveness Signaling	1.36E00	1.05E-01
Role of IL-17F in Allergic Inflammatory Airway Diseases	1.32E00	1.14E-01
Tryptophan Degradation to 2-amino-3-carboxymuconate Semialdehyde	1.32E00	2.5E-01

Table 3 Canonical Pathways enriched in GBM-EC differentially regulated genes.

Genes differentially expressed in GBM-ECs as compared to overall non-transformed EC transcriptome revealed significant enrichment of known and novel putative pathways within the GBM microenvironment ($p<0.05$ thought reported as –log(p-value)). The ratio is the number of genes in the pathway from our DEA divided by the total number of genes in that pathway.

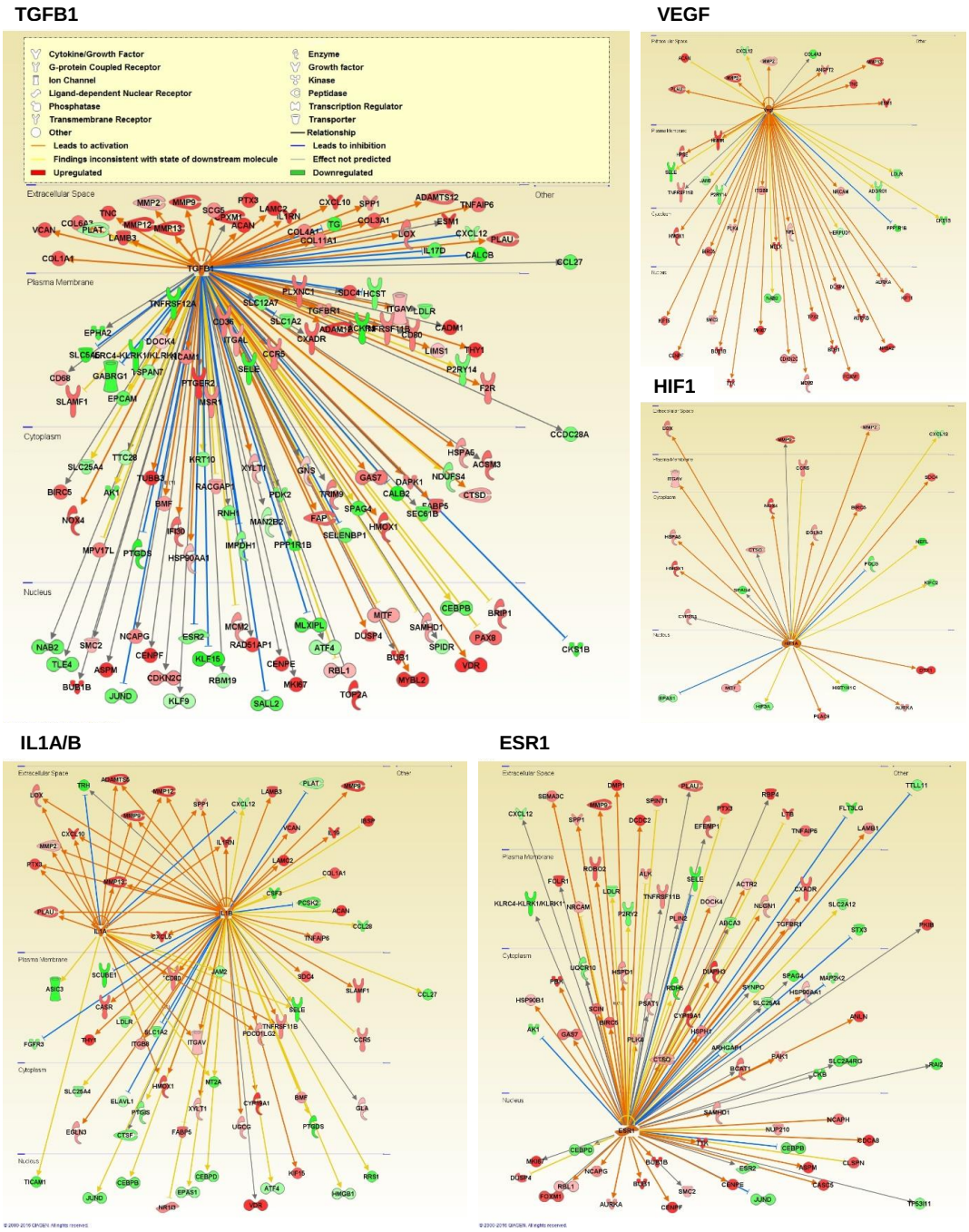

Figure 3 Select predicted to be activated Upstream Regulators of GBM-EC differentially regulated genes.

Genes differentially expressed in GBM-ECs as compared to overall non-transformed EC transcriptome predicted the activation of TGFB1, VEGF, HIF1a, IL1A and IL1B, along with ESR1 upstream regulators (z-score>2; $p<0.05$).

Generation of a GBM perivascular interactome of EC angiocrines acting on GMBSC signaling systems

Considering the functional relationship previously described between tumor-associated endothelial cells and GBMSCs (Calabrese et al., 2007; Veeravagu et al., 2008), we sought to identify the angiocrine signaling systems that mediate tumor propagation, as a first step to determine mechanisms of GBMSC dependence on the tumor perivascular niche. A putative GBMSC-EC interactome was thus developed by generating unique transcriptional profiles for the interaction of GBM microvascular ECs and GBMSCs. We began our analysis by scrutinizing the 113 GBM-EC extracellular factors and the 331 GBMSC plasma membrane (PM) proteins, exclusively, which were differentially regulated as compared to the non-transformed ECs and GPCs (GBM-EC extracellular factors DEA (a), and GBM-SC PM proteins DEA (b) are shown in Supplementary Spreadsheet 3). Utilizing a combination of manual and IPA software curation, focusing on previously reported direct and indirect protein-protein interactions we identified 24 interacting groups (Table 4), encompassing hormones, extracellular matrix components such as laminins, collagens, and matrix metalloproteinases, and members of the small integrin-binding ligand N-linked glycoprotein (SIBLING) family of proteins. In the case of the SIBLINGs, the interacting PM interaction partners are mostly those reported for the osteopontin (OPN) encoding gene, SPP1, though due to conservation of various functional motifs, such as post-translational modification motifs, acidic amino acids, and the RGD (Arg-Gly-Asp) motif (Bellahcene et al., 2008), we

extended the interaction unit to include all upregulated members of this family (distinguished in gray in Table 4).

This interactome, however, assumed that both the extracellular factors/ligands and the plasma membrane proteins/receptors must necessarily be dysregulated for their interaction to be of consequence in promoting tumor propagation. We next hypothesized that the dysregulation of one or the other (i.e. angiocrine or receptor) or simply the presence of any signaling pathways that may even be present in non-neoplastic EC-GPC interactions, once present in the anomalous tumor PVN, may contribute to GBM propagation. In order to obtain a more comprehensive view of all of the EC angiocrines expressed in the PVN and their putative interaction with all the GBMSC plasma membrane proteins, we utilized FPKM expression values (fragments per kilobase of transcript sequence per million mapped fragments) and considered FPKM>1 for at least 1/3 of the samples thus accounting for the heterogeneity that exists among GBMs. We thus identified 552 GBM-EC extracellular factors and 1254 GBMSC plasma membrane genes (GBM-EC extracellular factors FPKM (a), GBMSC PM proteins FPKM (b), and our comprehensive PVN interactome by FPKM expression units (c) are shown in Supplementary Spreadsheet 4, where FPKM>4 are highlighted in red and collagen and complement factor interactions are not shown). To elucidate the contribution of EC factors to GBMSC tumor propagation specifically, we then eliminated factors that were expressed by both GBM-ECs and GBMSCs with an FPKM difference of <4, thus narrowing the interactome to GBMSC dependence on ECs, and not GBMSC autocrine signaling. We identified 135 angiocrines that had at least one, but often multiple putative GBMSC interacting partners (Supplementary Spreadsheet 4c). Within

this comprehensive interactome, many of the previously reported PVN angiocrine-receptor interactions were present (Table 5). Furthermore, we identified multiple novel putative interactions, among which select cytokines, growth factors, Inhibins (representing a sub-group of the TGFβ protein superfamily), extracellular matrix components, as small leucine-rich proteoglycan (SLRP) family of proteins like Lumican and Biglycan, and basement membrane components, as Nidogen angiocrines, along with their putative binding partners are shown (Figure 4), demonstrating the complexity of the signaling systems contributing to GBM PVN. Interestingly, IPA analysis of the diseases and functions associated with this comprehensive interactome revealed a significant role for tumor cell movement, migration, and invasion (Table 6), along with proliferation and cellular generation.

GBM-EC angiocrine	GBMSC Receptors
SST	SSTR3
LTB	TNFRSF1A
SIBLING Family	ITGA5
SPP1	ITGA10
IBSP	ITGA2B
DMP1	ITGA8
MEPE	ITGA1
DSPP	ITGB7
	EGFR
IFNB1	IFNAR2
IFNE	IFNAR2
IL19	IL20RB
	IL20RA
ESM1	ITGAL
MBL2	TLR3
AMBP	CD79A
LAMC2	EGFR
LAMB1	ANTXR2
FRAS1	NPNT
	DLG4
ANOS1	FGFR1
FREM1	NPNT
COL1A1	KCNMA1
MMP9	ITGA5
	ITGAL
	NTRK1
CXCL12	ANXA2
	CXCR4
LGALS4	SLC9A3R1
ABI3BP	GRK5
MMP2	ITGA5
	ITGAL
PLAT	ANXA2
ANGPT2	ITGA5
SEMA3C	NRP2
HECW2A	LYNX1

Table 4 PVN interactome according to DEA.

Differentially regulated genes (as compared to non-transformed EC and GPC expression) with putative GBM-EC angiocrine-GBMSC receptor interactions are shown. In red are those upregulated and in green are those downregulated in their respective cell type. In grey are predicted interactions according to functional motif similarities among the angiocrines.

TGFB1	**TGFBR1**	TGFBI	AGRN	IGF2R	ITGAV	BMPR1A	ENG	ITGA3	ITGA5
	TGFBR2	ACVR1	ITGB3	TLR2	EGFR	LRP1	SCUBE3	SDC2	SDC4
IL6	**IL6R**	IL6ST	TNFRSF1A	TNFRSF1B					
DLL4	**NOTCH1**	NOTCH2							
SPP1/OPN	**ITGAV**	**ITGB1**	**ITGA5**	AMOTL2	BSG	CACNG4	MYD88	LRRC4	
	CD44	**ITGA4**	**ITGA9**	GRIPAP1	IFITM3	KCNIP1	MARCKS	NCKAP1	
	EGFR	**ITGB3**	CD151	NCSTN	SDC4	SLC39A6	SNAPIN	TBC1D8	
LAMA4	**ITGA6**	ITGA3	ITGAV	ITGB1	ITGB3	LGALS9	MCAM	PILRA	SDC4
LAMB1	**ITGA6**	ERBB2IP	ITGA3	ITGB1	LGALS9	PTPRK			
LAMC1	**ITGA6**	ITGA3	ITGA5	ITGAV	ITGB1	ITGB3	LGR4	SNAPIN	
CXCL12	**CXCR4**	ANXA2	ACKR3	SDC4	DPP4				

Table 5 Known PVN ligands and their putative interactions with GBMSCs within the comprehensive intractome according to FPKM expression units.

In bold are the GBM PVN ligand-receptor interactions previously reported in literature (reviewed in (Sharma and Shiras, 2016)).

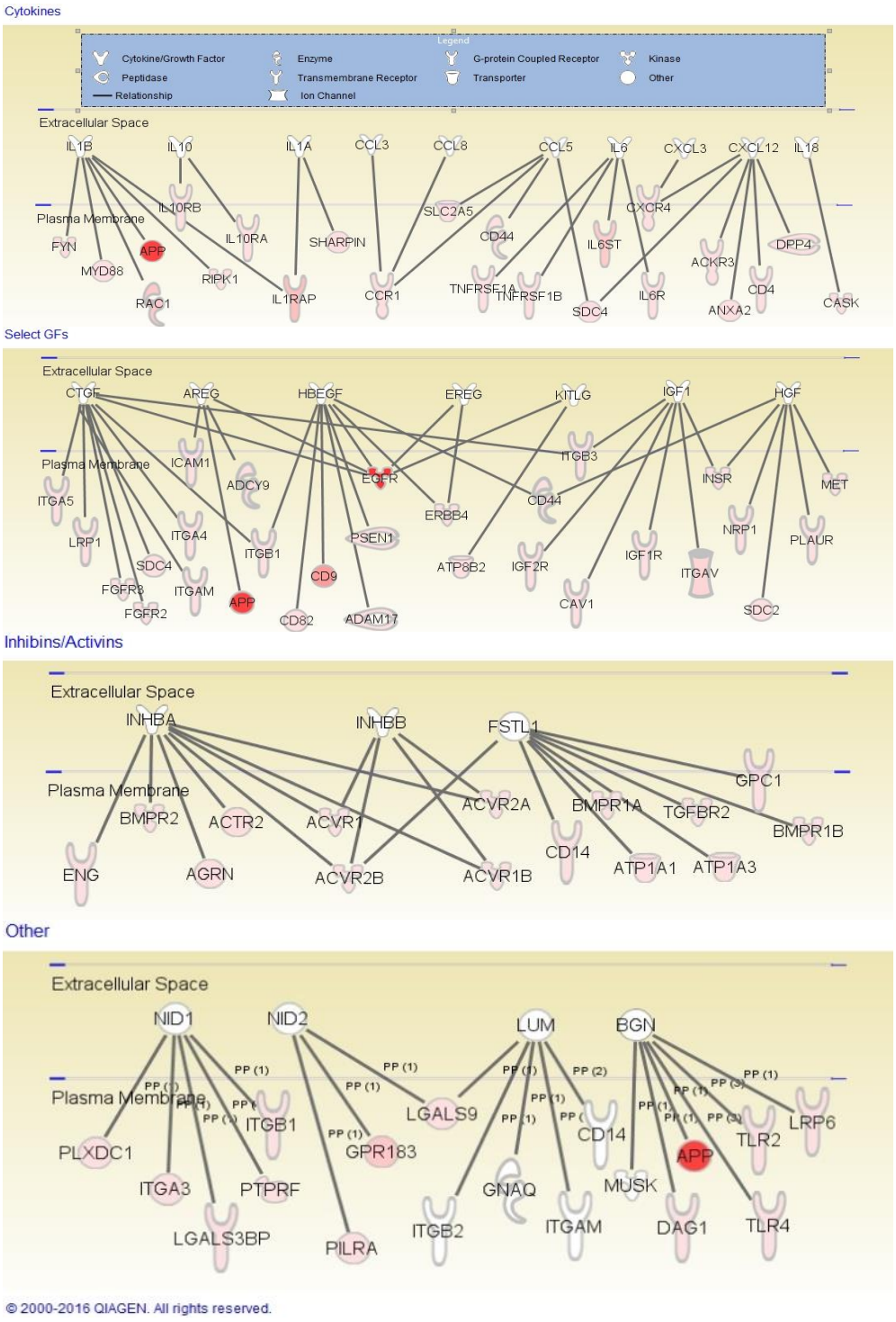

Figure 4 Select putative interaction groups within the comprehensive intractome.

From the top, select cytokins, growth factors (GFs), inhibits, and other exctracellular matrix/basement membrane GBM-EC expressed ligands and their potential interaction partners localized to GBMSC PM are shown. Receptors are shaded in a gradient from white to red according to increasing levels of expression.

Categories	Diseases or Functions Annotation	p-Value	# Molecules
Cellular Movement	migration of cells	3.67E-116	252
Cellular Movement	cell movement	1.08E-109	257
Cell-To-Cell Signaling and Interaction	binding of cells	1.15E-89	124
Cardiovascular System Development and Function, Organismal Development	angiogenesis	4.06E-88	162
Cardiovascular System Development and Function, Organismal Development	vasculogenesis	1.02E-87	148
Cellular Movement, Hematological System Development and Function, Immune Cell Trafficking	cell movement of leukocytes	3.23E-85	148
Cellular Movement, Immune Cell Trafficking	leukocyte migration	3.70E-83	154
Cellular Movement, Hematological System Development and Function, Immune Cell Trafficking	cell movement of myeloid cells	8.91E-79	122
Cell-To-Cell Signaling and Interaction	activation of cells	2.19E-78	156
Cardiovascular System Development and Function, Cellular Movement	migration of endothelial cells	1.03E-76	97
Cardiovascular System Development and Function, Cellular Movement	cell movement of endothelial cells	2.07E-75	99
Tissue Development	growth of epithelial tissue	6.89E-75	130
Cellular Growth and Proliferation	proliferation of cells	6.99E-75	284
Cellular Movement, Hematological System Development and Function, Immune Cell Trafficking, Inflammatory Response	cell movement of phagocytes	2.07E-74	119
Cellular Development	differentiation of cells	3.52E-74	224
Cellular Movement	homing of cells	9.70E-72	118
Cellular Movement	chemotaxis	2.47E-71	115
Cellular Movement	chemotaxis of cells	1.12E-70	113
Cellular Movement	migration of tumor cell lines	4.07E-70	130
Cellular Growth and Proliferation, Tissue Development	generation of cells	5.70E-70	208
Cellular Movement	cell movement of tumor cell lines	8.41E-70	140
Cell-To-Cell Signaling and Interaction	adhesion of blood cells	1.24E-68	96
Cell Death and Survival	cell death	1.49E-67	263
Cellular Movement, Hematological System Development and Function, Immune Cell Trafficking	cell movement of mononuclear leukocytes	1.82E-67	104
Tissue Morphology	quantity of cells	2.84E-66	190

Table 6 Diseases and Functions significantly associated with all angiocrines and their putative GBMSC PM interaction partners from the comprehensive interactome.

The top 25 most significantly associated functions with the molecules of the intractome according to FPKM expression units are shown, along with the number of molecules from our list used for these predictions.

Integrin-Binding Sialoprotein (IBSP): a highly expressed and significantly upregulated angiocrine identified by the perivascular niche interactome

Within the PVN interactome multiple SIBLING family members were expressed, and were highly upregulated GBM-EC factors as compared to non-transformed ECs (Table 7). IBSP was almost exclusively expressed by the tumor ECs (FPKM=50.1 vs. GBMSC FPKM=2.4; Supplementary Spreadsheet 4c) and was the most upregulated member of this family with logFC of 13 (Table 7, in red, p=0.0001). SPP1, the gene encoding the well-studied OPN that has been shown to have a role in various stages of cancer progression (Bellahcene et al., 2008), was not upregulated to the extent of IBSP (logFC of 3) by GBM-ECs, and was also expressed at high levels not only by tumor ECs (FPKM=664) but also by the GBMSCs (FPKM=114.7; Supplementary Spreadsheet 4c). Other member of this family, though upregulated, were not highly expressed (FPKM<4) and thus may not have as significant of a role as OPN and IBSP in GBM tumor propagation. Putative SIBLING receptors from our interactome according to GBMSC FPKM expression units are also shown in Table 7, and consist mainly of integrin receptors (ITGs), which are shown to interact with the RGD domain of SIBLINGs in various normal and neoplastic tissues (Bellahcene et al., 2008). IBSP vascular expression was confirmed by immunohistochemistry (IHC) with intense staining of the vessels in multiple primary GBM samples, and general staining of the extracellular space within the tumor-rich areas of the tissue (Figure 5A). GBM4 and GBM11 were samples used in our RNA-seq study, and HK217 was a sample whose primary gliomasphere line was used in many of our functional assays. Endothelial expression of

IBSP was also confirmed by immunofluorescent (IF) co-staining of von Willebrand factor (VWF) and with IBSP (Figure 5B). Using the TCGA gene expression data on GBMs (2008), and examining one standard deviation from the mean, low IBSP expression correlated with increased GBM patient survival ($p=0.0003$; Figure 5C). We also utilized the open-access GlioVis tools (http://gliovis.bioinfo.cnio.es/) to assess GBM patient survival correlation with IBSP expression. At high vs. low quartile cutoffs for Kaplan-Meier survival plots, TCGA dataset survival correlation with IBSP expression did not reach significance (Figure 5D, top panel), but the Rembrandt GBM dataset (Madhavan et al., 2009) did demonstrate a significant survival disadvantage with IBSP enrichment (Figure 5D, bottom panel; $p>0.05$), in line with the previously reported IBSP expression correlation with poor GBM patient prognosis (Xu et al., 2012).

gene	Small integrin-binding ligand N-linked glycoprotein (SIBLINGs) Family of proteins	FPKM GBMEC	Enrichment Factor (LogFC vs. Normal Endothelial Cells)	P-Values	Candidate GBMSC Receptors
SPP1	secreted phosphoprotein1 (Osteopontin)	663.62	3	0.0008	ITGAV ITGB3 ITGB1 ITGB5 ITGA6 ITGA9 ITGB8 ITGA1 ITGA7 ITGA5 CD44
IBSP	**integrin-binding sialoprotein**	**50.09**	**13**	**0.00001**	
DMP1	dentin matrix acidic phosphoprotein 1	3.22	8	0.002	
DSPP	dentin sialophosphoprotein	3.21	6	0.008	
MEPE	matrix extracellular phosphoglycoprotein	3.30	4	0.004	

Table 7 SIBLING upregulation and FPKM expression units in GBM-ECs.

All members, except DSPP, were significantly upregulated as compared to non-transformed ECs ($p<0.005$). IBSP is highlighted in red as the most highly upregulated member of this family as compared to non-transformed ECs. SIBLING putative receptors are taken from the comprehensive interactome according to FPKM expression units.

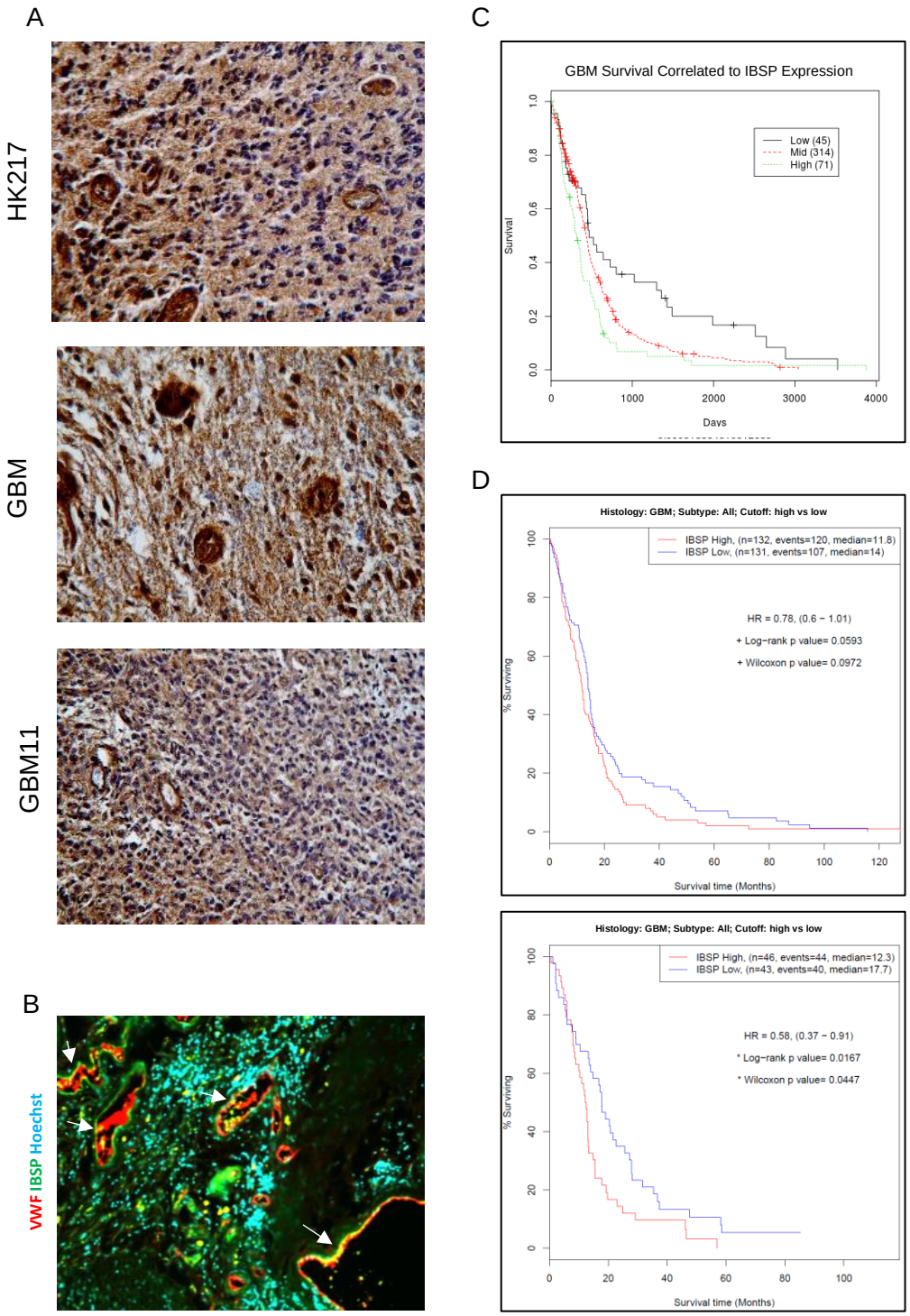

Figure 5 IBSP GBM-EC expression confirmation and correlation with poor patient survival.

(A) IHC staining of IBSP with dark vascular staining in three primary GBM samples and diffuse extracellular matrix staining. (B) IF staining of IBSP (green), VWF (red), and Hoechst (blue) in a primary GBM sample. White arrows are pointing to co-staining of VWF and IBSP (yellow). (C) Kaplan-Meier survival plot of mean IBSP expression ± one standard deviation using TCGA GBM dataset. Low expression correlated with increased survival ($p<0.0005$). (D) GlioVis generated Kaplan-Meier plots of IBSP high vs. low expression (quartiles) correlated to patient survival utilizing the TCGA GBM dataset (top), and the Rembrandt GBM dataset (bottom). Only the Rembrandt data demonstrated that significantly poorer survival correlated with high IBSP expression ($p<0.05$) using the high vs. low quartile cutoffs.

IBSP is an adhesion molecule with low expression level in gliomasphere cultures that correlated negatively with sphere formation

GBMSCs, similar to neural stem cells (NSCs), have the capacity for self-renewal and proliferation over multiple passages *in vitro*, and are enriched in serum-free gliomashere culturing conditions, virtually identical to those used in culturing neurospheres (Galli et al., 2004; Hemmati et al., 2003). GBM-derived primary human gliomasphere cultures exhibit multipotency in terms of giving rise to a heterogenous mixture of cells that are representative of the original tumor, and *in vivo* xenotransplantation of GBMSC-enriched cell populations lead to tumors that have similar characteristics of the original patient tumor (Galli et al., 2004; Hemmati et al., 2003; Nunes et al., 2003; Rich and Eyler, 2008; Singh et al., 2004). Our lab recently published a large-scale analysis of gliomasphere expression and functional data (Laks et al., 2016). As expected, based on the comprehensive interactome's cell-type specific expression patterns of the SIBLING proteins, unlike Osteopontin, IBSP expression in the gliomasphere lines was very low (Figure 6A, N=70). Since OPN was previously shown to promote glioblastoma sphere formation as a measure of tumorigenicity, *in vitro* (Lamour et al., 2015), we next examined the gene sets that were significantly correlated with sphere forming capacity within our library of gliomasphere lines (Laks et al., 2016), and found concordance with this finding, as OPN expression was significantly and positively correlated with sphere formation (Pearson correlation coefficient r=0.4). Conversely, IBSP expression was much more significantly and negatively correlated with sphere forming capacity (r=-0.72; Figure 6B). Since induction of adhesion is a major contribution of IBSP in breast and prostate cancer progression (Gordon et al.,

2009; Sung et al., 1998), we wondered whether a similar effect may also be contributing to the reduced sphere formation capacity of the gliomashperes with higher IBSP expression, as they would prefer to form a monolayer instead of spheres in the 3D culture. We thus treated freshly dissociated gliomaspheres with 250nM IBSP and observed a robust adhesion function on gliomasphere cultures in presence of this soluble secreted glycoproteins (Figure 6C).

A

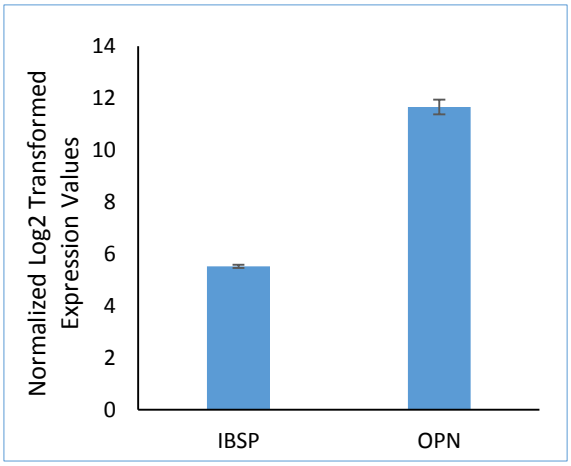

B

Gen by Gene Correlation Significantly (P<0.001) Associated with Sphere Formation				
Probe	Symbol	Description	Pearson correlation	P-Value
212222_at	IBSP	integrin-binding sialoprotein	-0.72	1.7E-12
226513_at	SPP1	Secreted phosphoprotein 1	0.40	5.6E-04

C

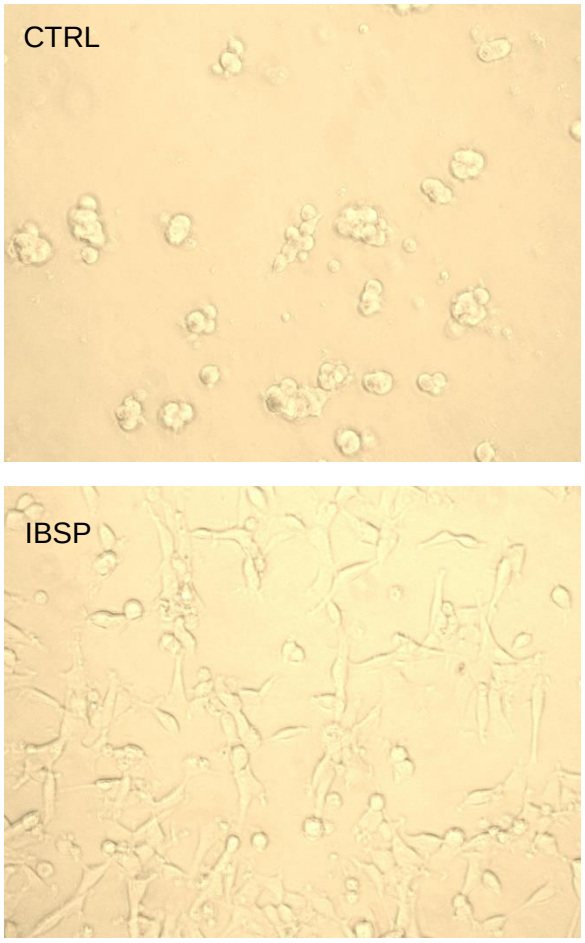

Figure 6 Endogenous and exogenous IBSP effect on gliomasphere cultures.

(A) Endogenous expression of IBSP as compared to OPN in primary human gliomasphere cultures (N=70). (B) Gene expression-phenotype correlation in a gene-by-gene correlation analysis, showing IBPS and SPP1 correlation coefficients of -0.72, and 0.40 with sphere formation, respectively ($p<0.001$). (C) HK217 gliomasphere primary GBM line grown in absence (CTRL; top panel), or presence of 250nM IBSP (bottom panel) for two days.

IBSP promoted gliomasphere-derived GBMSC migration and invasion within 3D biomimetic hydrogel-based physiologically relevant microenvironments

Along with the reported and observed adhesion function of IBSP, it has been shown to induce tumor cell invasion properties through its interactions mainly with ITGαV containing integrin receptors (Gordon et al., 2009; Sung et al., 1998). We thus wondered if IBSP may also contribute to the cellular movement, migratory capacity, and the invasive role of GBMSC-EC PVN interactome as predicted by IPA. We utilized unique hyaluronic acid (HA)-based hydrogels as *ex vivo* culture systems that simulated the mechanical stiffness of the brain (Seidlits et al., 2010), and the HA-rich GBM chemical composition (Jadin et al., 2015). HK217 GBM-derived gliomaspheres were encapsulated within these biomimetic environments in the absence of any peptide (where a Cysteine amino acid reacts from thiol to the vinyl sulfone; see Experimental Procedures), in presence of an integrin-binding RGD containing peptide of the IBSP proteins “GGGNGEPRGDNYRAY” (IBSP), a 3-amino acid RGD peptide (RGD), or an IBSP-RDG control peptide (IBSP-RDG CTRL), which consisted of the same flanking regions as the IBSP peptide, but with a scrambled integrin-binding domain (Figure 7A). As can be seen, and quantified (N≥8, Figure 9B), within the first hour of encapsulation, which is the remaining time required for the gelling of the environment, IBSP and RGD peptides both induced diffuse sphere borders. Interestingly, by Day3 the IBSP peptide caused an average migration distance of 204.1±10μm (N=14) from the sphere edge/front in HK217, which was substantially greater than even the induction of invasion by the RGD peptide (62.6±6μm; N=8). Little extension or dispersion of the GBMSCs from the encapsulated gliomaspheres was seen in the Cystein or the IBSP-RDG CTRL

hydorgels (Figure 7B). Similar effects of the IBSP peptide were shown for another primary gliomasphere line (Figure 9), although images shown are from Day6 post encapsulation, as HK301 required a longer period of time to exhibit its migratory potential, possibly due to inherent GBM heterogeneity. Nevertheless, in both primary cell lines the IBSP peptide significantly increased the migration of the cells lining the periphery of the spheres at compared to IBSP-CTRL (HK217) or Cys (HK301) ($p<5e-5$, and 5e-11, respectively). This phenotype may be similar to the glioma tumor progression of human neoplasms, in which proliferative tumor cores give rise to highly migratory, and thus diffuse tumor borders.

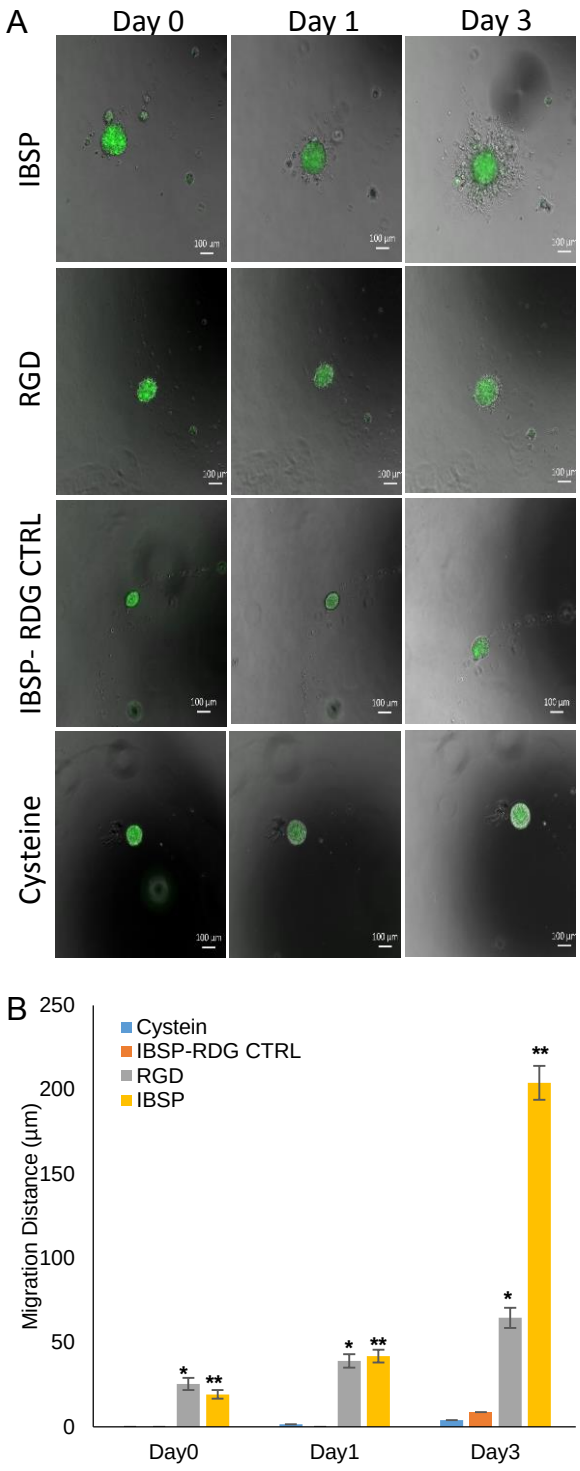

Figure 7 The IBSP peptide promoted HK217 migration in hydrogel-based microenvironment.

(A) Representative images of a sphere encapsulated in various hydrogel conditions (vertical axis) imaged over three days (horizontal axis). Endogenous reporter (green). (B) Quantification of migration distance from sphere edge over three days. Cysteine N=9, IBSP-RDG CTRL N=8, RGD N=8, IBSP N=14. * RGD compared to Cysteine $p<1e-6$, **IBSP compared to IBSP-RDG CTRL $p<5e-5$, one-tailed unpaired Student's t test.

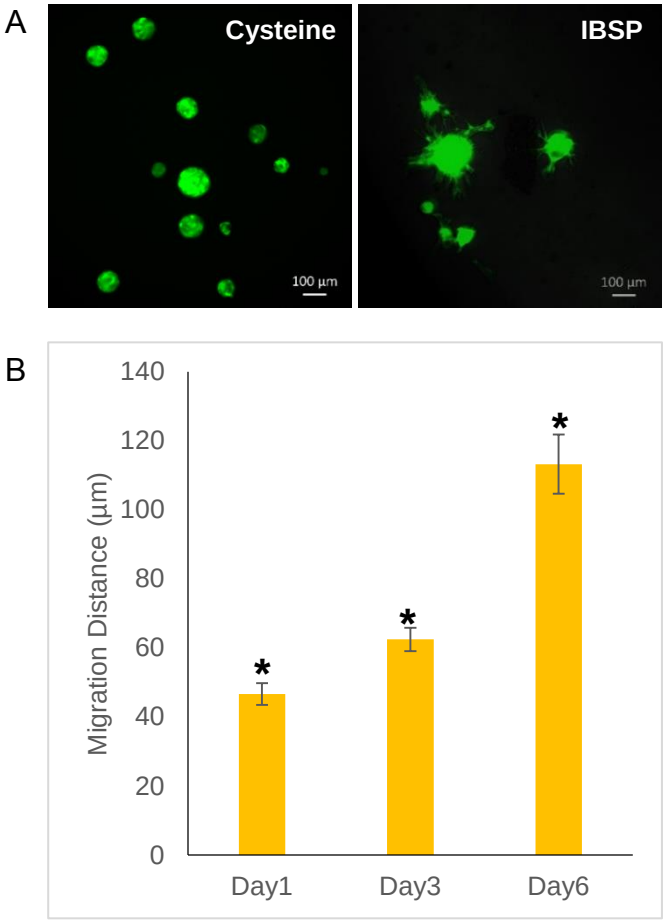

Figure 8 HK301 gliomaspheres verified the migration-inducing properties of IBSP.

(A) Representative images of spheres in 3D hydrogel-based microenvironments 6 days post encapsulation in absence (Cysteine) or presence of the IBSP peptide. Endogenous reporter (green). (B) Quantification of the migration distance from the sphere edge over six days, shown only for IBSP (N=11 Day 1, N=13 Day 3, and N=9 Day 6), since spheres encapsulated in the Cysteine gels showed no cell migration from sphere edge at any time point, i.e. 0 µm for N=10 analyzed at each time point. *IBSP compared to Cysteine $p<5e-11$, one-tailed unpaired Student's t test.

An shRNA screen of GBMSC receptors allowed for identification of specific ITGs responsible for IBSP's action on GBMSC migratory capacity

Since the RGD domain of the IBSP was necessary for increasing the migratory capacity of gliomasphere GBMSCs, we next wondered which ITGs were responsible for the IBSP action on GBMSCs. From the comprehensive interactome, we identified a number of expressed ITGs (Table 7), some of which were previously shown to interact with the SIBLING ligands in other cancers. For example, ITG αVβ3 and αVβ5, respectively, interact with IBSP to promote breast cancer proliferation, and invasion (Sung et al., 1998). In order to utilize interfering RNA technologies to investigate the GBMSC receptor side of this interaction, however, we first developed a high-throughput (HT) method to assess cellular dispersion in our 3D microenvironments (detailed in Experimental Procedures), and verified our previous migration results in this new experimental paradigm using HK217 (Figure 9). The quantification of migration/invasion capacity was measured as the number of objects dispersed per gel (Figure 9B). As expected, in the presence of the IBSP peptide, a significantly larger number of objects were dispersed from the spheres as compared to Cysteine or IBSP-RDG CTRL conditions ($p<0.01$). We then carried out a loss-of-function short hairpin-lentiviral RNA screen of the 11 receptors of interest, by assessing 36 different knockdown (KD) clones, and observed that no single ITG KD completely rescued the invasive phenotype that was induced by the IBSP peptide (Figure 10). Infection with at least one of the clones for ITGαV, ITGβ3, ITGα6, ITGα7, ITGβ8, and ITGα1 resulted in significantly reduced GBMSC dispersion in hydrogel ($3\leq N\leq 8$). Of these genes, ITGβ8 and ITGαV were the highest expressing GBMSC ITGs (average FPKM values of of 82.9 and 31.3,

respectively). A clone of ITGβ1 KD, also significantly increased GBMSC dispersion (84±42).

In light of our screen results, and the considerable reported role of ITGαV containing heterodimers in cell invasion and migration (Hood and Cheresh, 2002), we also assessed gliomasphere GBMSC migratory potential in hydrogels in presence of ITGαV specific blocking antibodies, L230 and 17E6 (Figure 11). HK217 GBMSCs were pre-treated with the antibodies for four days before small gliomaspheres were encapsulated in hydrogels. Once gelled, complete NS media containing 10μg/ml of each blocking antibody was added to ensure continued inhibition of ITGαV integrins. Though 17E6 is reported by the manufacturer to block all ITGαV integrins, L230 recognizes heterodimers αVβ3, αVβ1, αVβ5 and αVβ6, specifically. At 2 days post encapsulation both blockers inhibited the extent of IBSP-induced GBMSC migration and invasion away from the gliomasphere core. However, 17E6, completely abrogated such cellular movement, whereas L230 displayed uneven sphere edges and some extending of the gliomasphere peripheral GBM cells (Figure 11). Combining the results from our screen, the expression levels of the various ITGs on GBMSCs, and the experimental outcome of inhibiting ITGαV specifically, we posit that endothelial IBSP migratory action on GBMSCs is most likely the result of its interaction with ITGαV integrin, including ITGαVβ8, as having the highest GBMSC expression. Though IBSP interacts with other heterodimers, it possibly does so to a lower extent, and/or other ITGs' lower expression levels may render them less important in IBSP regulation of GBMSCs.

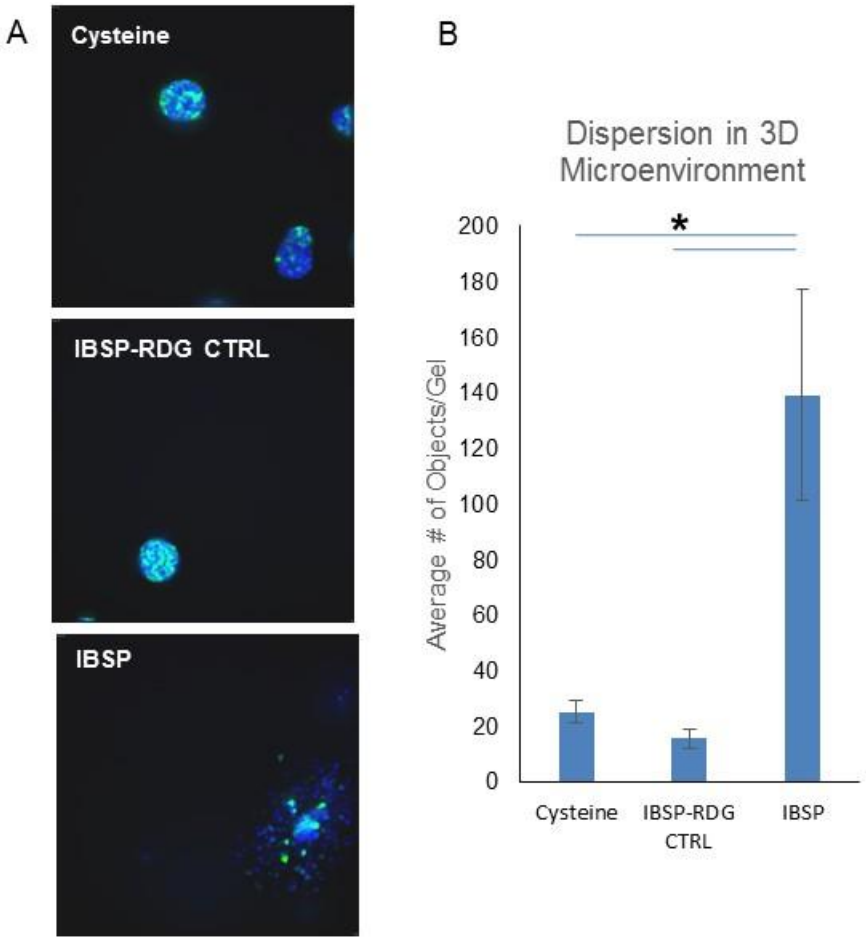

Figure 9 An HT method to assess cellular dispersion in hydrogel microenvironments.

(A) HK217 cells encapsulated in Cysteine, IBSP-RDG CTRL or IBSP peptide hydrogel conditions in a 384-well plate at day 3 post encapsulation. Endogenous reporter (green), Hoechst (blue). (B) Quantification of the average number of objects detected by the analysis software (see Experimental Procedures) per gel. * $p<0.01$ one-tailed unpaired Student's t test.

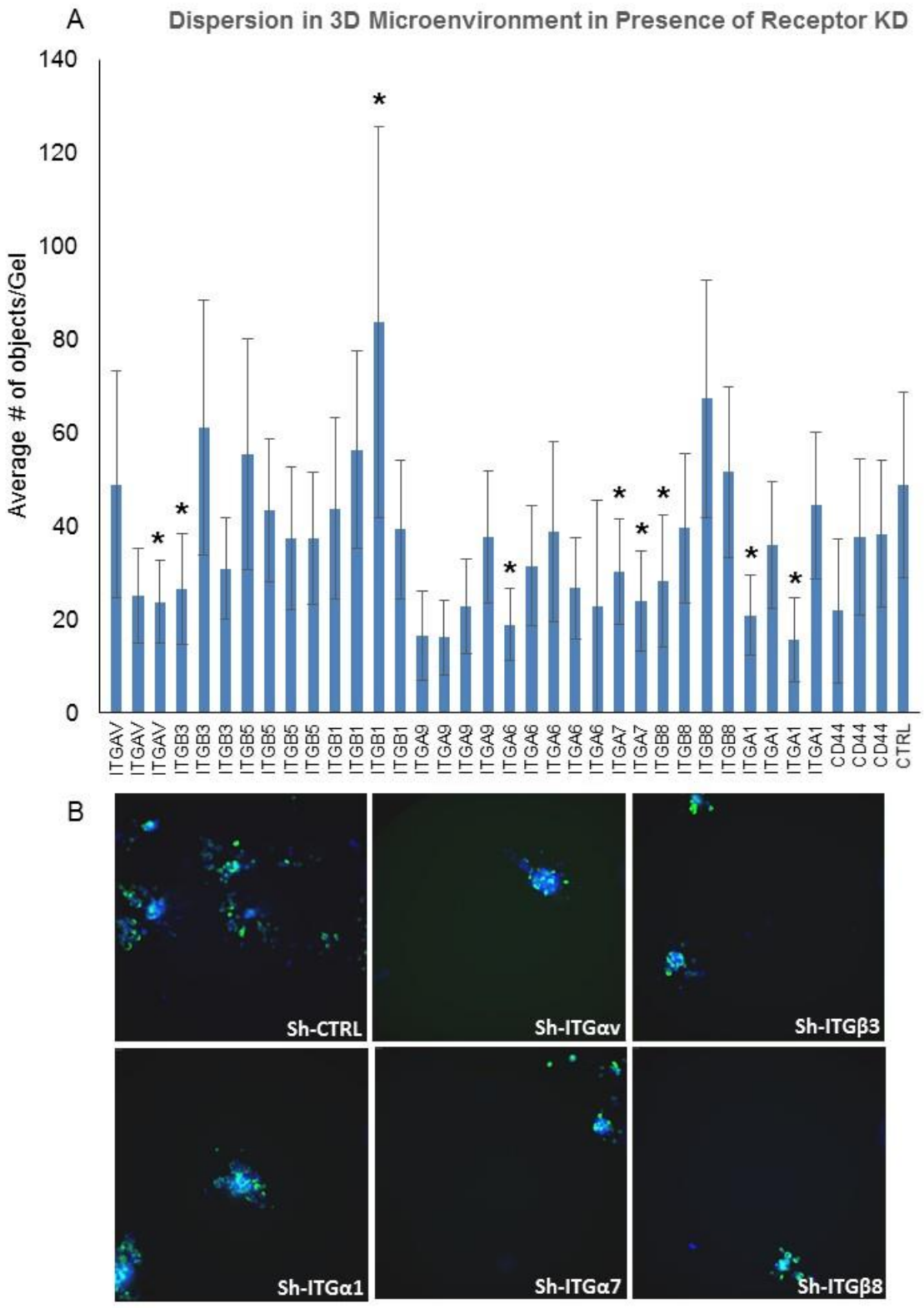

Figure 10 An shRNA screen of GBMSC receptors revealed ITGs mediating IBSP action

on GBMSC migratory capacity.

(A) Quantification of the average number of objects detected per gel. All conditions were in presence of the IBSP peptide, where CTRL designates a reporter lentivirus without any receptor KD. All KD condition comparisons were to CTRL. *$p<0.01$ one-tailed unpaired Student's t test. (B) Representative images of various shRNA clones which displayed significantly reduced object dispersion within the hydrogel as compared to CTRL.

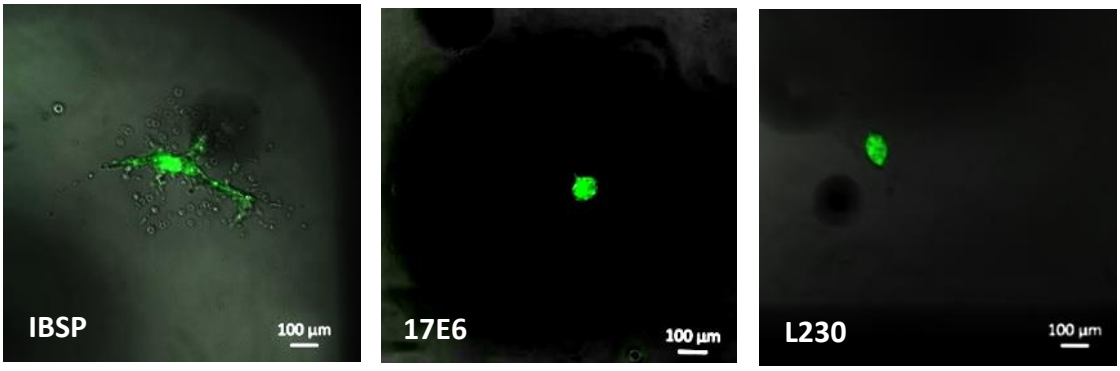

Figure 11 ITGαV antibody blockers abrogated IBSP migratory action on gliomaspheres.

Spheres treated and encapsulated with L230 displayed diffuse borders whereas those treated with 17E6 showed complete inhibition of migration.

IBSP selectively promoted proliferation of the Proneural gliomasphere cultures and its high expression is an indicator of poor patient survival in this subclass of GBMs

Though increased cellular movement, migration, and invasion were the most prominent functions of the PVN interactions, a significant role in proliferation and generation of cells was also revealed by the GBMSC-EC interactome (Table 6). Furthermore, both OPN and IBSP have been shown to promote cell survival and proliferation in other cancers (Bellahcene et al., 2008; Gordon et al., 2009; Sung et al., 1998). We thus wondered whether GBM cells grown in gliomasphere cultures in presence of IBSP would display increased proliferative capacity. Surprisingly, only gliomasphere cultures classified as Proneural (Laks et al., 2016), demonstrated significantly increased cell numbers with a 7day IBSP treatment (Figure 12), although only non-IDH1 mutant cultures were tested. To determine whether this increase was due to improved survival or enhanced proliferative capacity, we carried out 5-bromo-2'-deoxyuridine (BrdU) treatment of the IBSP-treated cells and observed an increased number of proliferating cells. Furthermore, interrogating GBM patient survival data according to TCGA subclassifications from both the TCGA and Rembrandt GBM transcriptome datasets (2008; Madhavan et al., 2009), both accessed through GlioVis, revealed that Proneural GBMs were the only subclass with a significant correlation ($p<0.05$) between poor survival and high IBSP expression (Figure 13A-TCGA; Figure 13B-Rembrandt GBM databases).

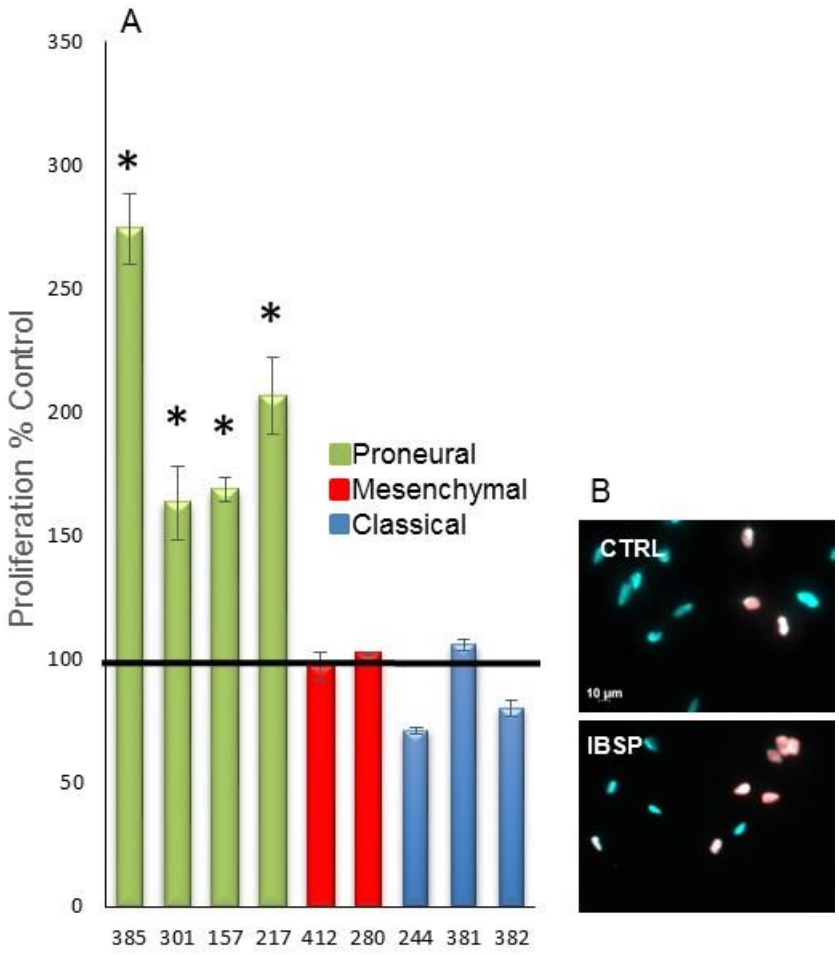

Figure 12 IBSP promoted PN gliomasphere proliferation.

(A) Cell counting assay as a measure of proliferation in various HK lines. Gliomasphere TCGA classifications are according to (Laks et al., 2016). *****$p<0.05$ one-tailed paired Student's t test. (B) BrdU immunolabeling of HK217 ± 2 day IBSP treatment.

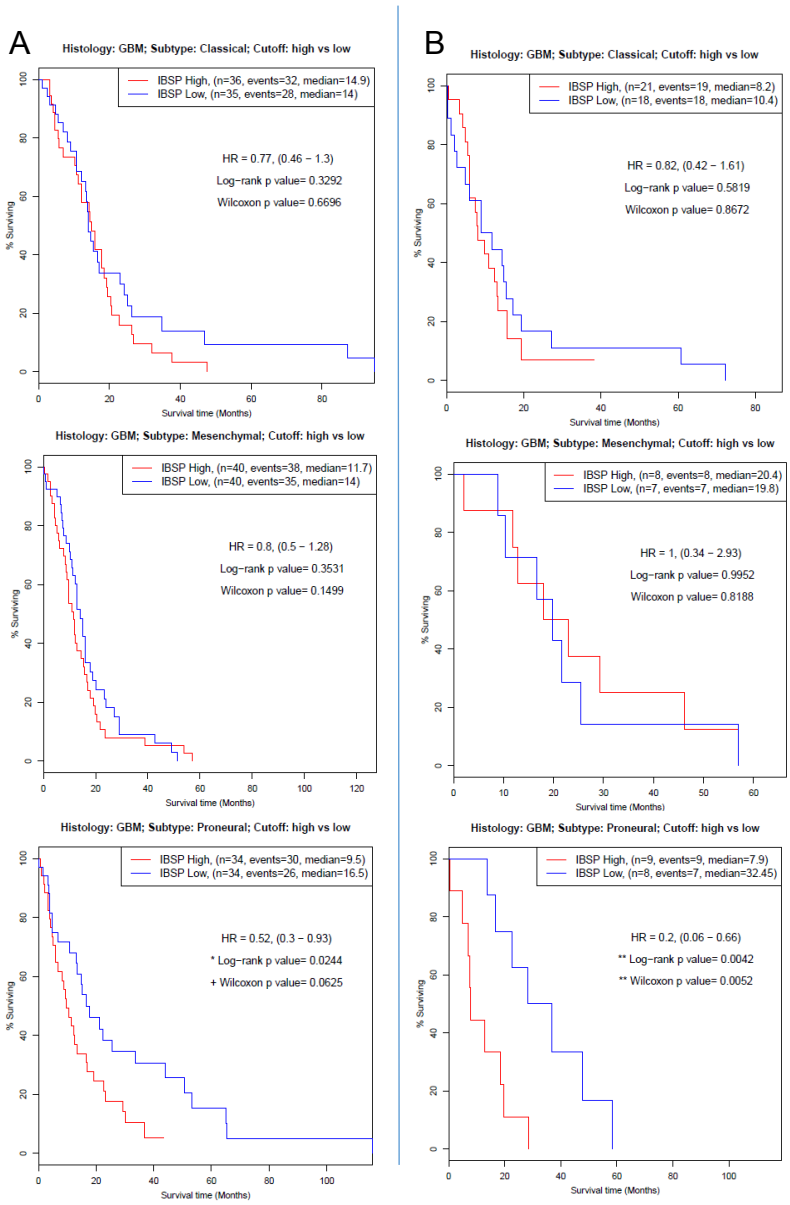

Figure 13 IBSP expression correlates with reduced patient survival in only PN GBMs.

Kaplan-Meier plots of patient survival correlation with IBSP gene expression in (A) TCGA database, (B) Rembrandt database, both showing samples with GBM histology only with high vs. low quartile cutoffs.

Promotion of a Proneural to Mesenchymal transformation gene expression signature by IBSP

Resembling the epithelial to mesenchymal transition, GBMSCs undergo a Proneural to Mesenchymal transformation accompanied by the enrichment of the cancer stem cell marker, CD44, along with NF_KB activation (Bhat et al., 2013). This transition may also be regulated by various transcription factors including C/EBPβ and STAT3 (Carro et al., 2010), and environmental conditions such as hypoxia, where the consequent HIF1α activation has been shown to promote GBM migration, and Mes transformation (Joseph et al., 2015). Though it is speculated that microenvironmental secreted factors may promote such a transformation of GBMSCs to acquire the more aggressive and invasive mesenchymal phenotype (Phillips et al., 2006), few if any such factors have been identified to date.

Microarray gene expression profiling of PN gliomasphere primary cell lines, HK157 and HK217, grown in the absence (CTRL) or presence of IBSP for 4 days revealed a dysregulated gene signature that accompanied the IBSP-induced proliferative and migratory phenotypes (Complete overall IBSP vs. CTRL DEA, FDR<0.001 (a), significantly enriched canonical pathways, p<0.05 (b), upstream regulators, p<0.05 (c), and diseases and functions associated with DEA, p<1.5e-6 (d) can be found in Supplementary Spreadsheet 5). Interestingly, IBSP significantly induced the canonical Mesenchymal gene, CD44 expression by 1.8-2.8 folds across 8 microarray probes (Supplementary Spreadsheet 5a), and the IPA-predicted increased functions associated with the set of dysregulated genes were mainly to promote tumor invasion and migration (Supplementary Spreadsheet 5d). Among the upregulated

genes, was also Matrix metalloproteinase2 (MMP2; FC=2.3, p=2.7e-11), which is upregulated and activated by IBSP in other cancers (Bellahcene et al., 2008; Gordon et al., 2009; Hwang et al., 2009), and has a well-studied role in promoting glioma invasion (Fillmore et al., 2001). Furthermore, the mesenchymal mode of GBM migration has been characterized by interaction of focal adhesion contacts between the extracellular matrix and ITGs through activation of the Focal Adhesion Kinase (FAK), and its downstream signaling pathways (Cha et al., 2016). Canonical Pathway analysis of the most significantly dysregulated genes revealed a significant enrichment of FAK, and integrin signaling pathways, as expected from our functional data, along with a significant role in glioma invasiveness signaling similar to genes significantly dysregulated in GBM-ECs vs. non-transformed ECs (Figure 14; Supplementary Spreadsheet 5b). The gene expression signature also revealed other pathways such as Paxillin, IGF-1, and Ephrin receptor signaling, which may play a role in a perivascular niche-induced acquisition of a more aggressive and invasive phenotype by GBM cells. Furthermore, IPA upstream regulator analysis predicted that NF_KB complex was significantly activated (z-score=3, p=4e-8; Figure 15A), accompanied by predicted activation of upstream regulators STAT3 (z-score=2.6, p=1.1e-6; Figure 15B) and HIF1α (z-score=2.4, p=3.8e-5; Figure 15C; Supplementary Spreadsheet 5c). C/EBPβ, though predicted as a significant upstream regulator (p=2.3e-5), had a z-score of 1.6, which was below the “prediction of activation state” cutoff (-2>z-score>2) in our analyses.

To further assess whether IBSP induced a PN to Mes transition, we classified the CTRL and IBSP treated cells according to TCGA classification of gliomaspheres (Laks et al., 2016) (Figure 16A), and examined their gene expression signatures as compared

to the tumors in the TCGA database. As expected, when we performed principal component analysis of genes used to categorize samples of the tumors in the TCGA database (2008; Verhaak et al., 2010), these samples separated according to subclass. We then superimposed the gene expression signatures of our control and treated gliomasphere samples (Figure 16B). This superimposition clearly demonstrated the movement of the samples from a more PN signature towards a more Mesenchymal signature upon IBSP treatment for both cell lines, particularly when comparing each CTRL to its paired IBSP sample. Though HK157 exhibited a more robust phenotype, HK217 did display a similar expression profile upon IBSP treatment as HK157, since its DEA (FDR<0.05) significantly overlapped with the HK157 DEA (p-Value of overlap=1.3e-243).

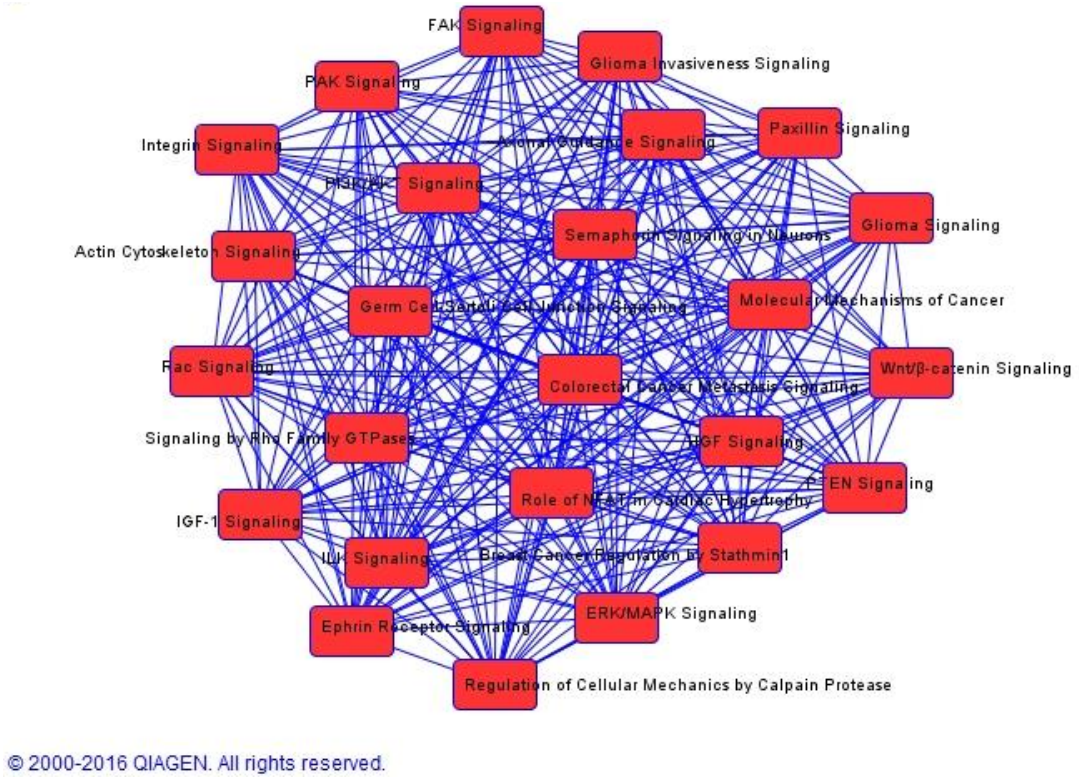

Figure 14 Overlapping canonical pathways significantly enriched by IBSP treatment as predicted by IPA.

The complete list of pathways and the molecules contributing the predictions can be found in Supplementary Spreadsheet 5b. $p<0.05$.

A: NFkB Complex

B: STAT3

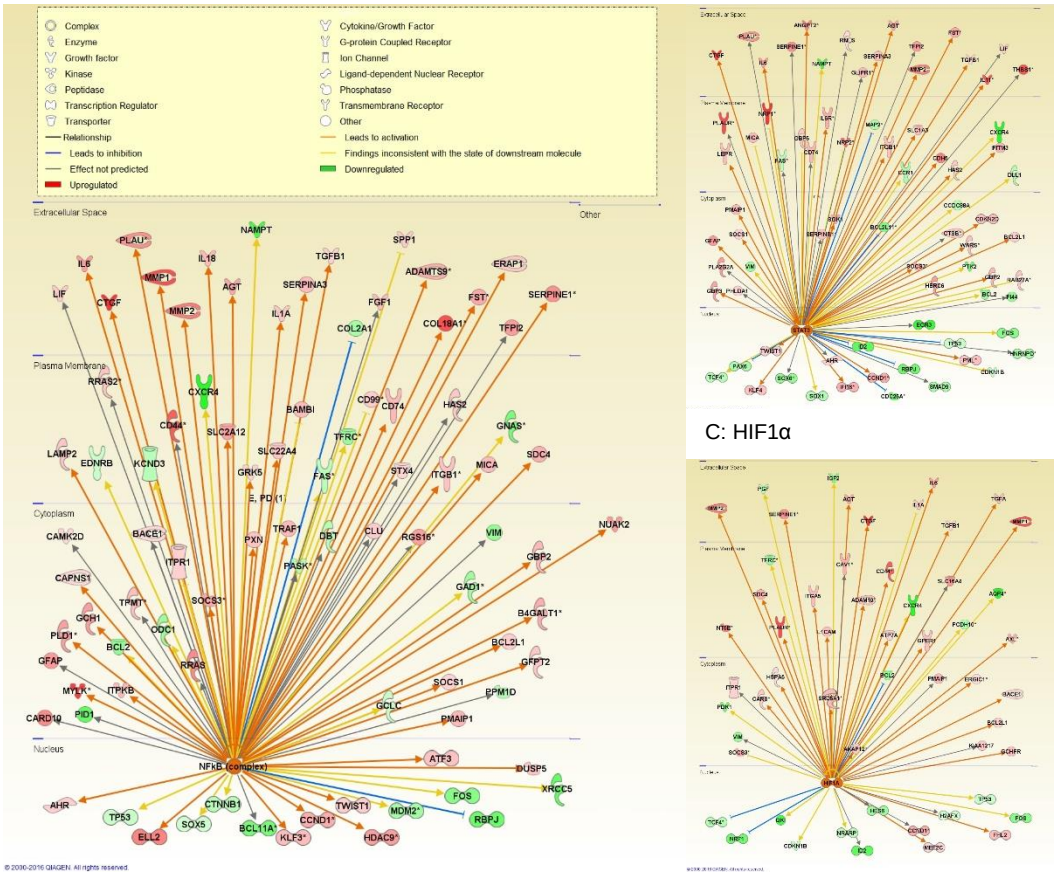

C: HIF1α

Figure 15 Multiple known Mesenchymal pathway regulators were also significantly activated upstream regulators of the IBSP-induced set of dysregulated genes.

NF_KB Complex (A) STAT3 (B) and HIF1α (C) activations were predicted based on the dysregulated molecules and relationships shown. All molecules were significantly dysregulated (FDR<0.001) and the p-Value of overlap, between our set of dysregulated genes and a given pathway's signaling molecules, was <0.05.

A

Sample	Prediction	Sample	Prediction
CTRL_157_4D_1	Proneural	CTRL_217_4D_1	Classical
CTRL_157_4D_2	Classical	CTRL_217_4D_2	Proneural
CTRL_157_4D_3	Proneural	CTRL_217_4D_3	Proneural
IBSP_157_4D_1	Mesenchymal	IBSP_217_4D_1	Mesenchymal
IBSP_157_4D_2	Mesenchymal	IBSP_217_4D_2	Classical
IBSP_157_4D_3	Mesenchymal	IBSP_217_4D_3	Classical

B

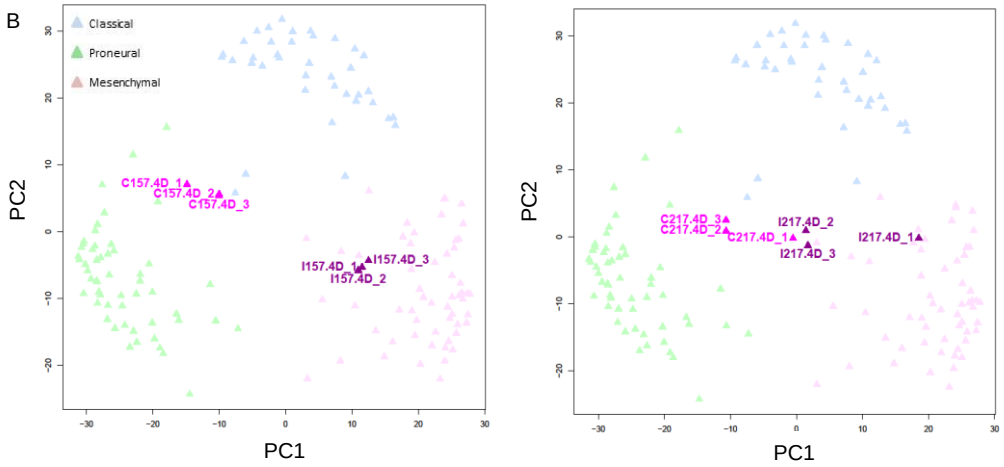

Figure 16 IBSP promoted a Mesenchymal expression signature.

(A) Predicted TCGA subclass of control (CTRL) or IBSP treated (IBSP), HK217 and HK157 lines. Cells were treated for 4 days. (B) PCA of GBMs in the TCGA database (in background) and our HK157 (left panel) and HK217 (right panel) gliomaspheres (CTRL in pink, IBSP in purple), distributed according to gene signature used in their TCGA classifications.

IBSP pre-treatment induced lasting functional changes and increased radioresistance in gliomaspheres

We set out to determine mechanisms of GBMSC dependence on vascular secreted factors. However, the expression and phenotypic changes induced by IBSP may have revealed a mechanism not only for GBM-EC maintenance of GBMSC stem-like characteristics, but also one through which, GBMSCs may gain independence from the perivascular niche, as they assume a more aggressive character. We thus carried out IBSP removal assays to determine whether this ligand's interactions with GBMSCs and the differential expression profiles it induced may promote lasting cellular functional change, which may contribute to a more aggressive tumor propagating phenotype. We observed that upon a 7 day IBSP pre-treatment, followed by dissociation of the spheres into single cells, and removal of the ligand from the culture media, HK157 gliomasphere cells continued to exhibit significantly increased proliferative potential at 148±11% that of cells not previously treated (Figure 17). Furthermore, exposing these cells to a 4 Gray (Gy) dose of ionizing radiation upon removal of the ligand demonstrated significantly increased radiation resistance in the cells previously treated with IBSP (Figure 17). The control cells' proliferation decreased to 31.4±0.8% of non-irradiated, non-treated cells, and IBSP-treated cells' proliferation decreased to 44.7±1.2% of the non-irradiated previously-treated cells (data not shown). Thus IBSP pre-treatment promoted a more radioresistant phenotype, which did not depend on the continuous presence of the ligand. This phenotype may be attributable to the proposed Mesenchymal transition, which has been shown to promote radiation resistance (Bhat et al., 2013).

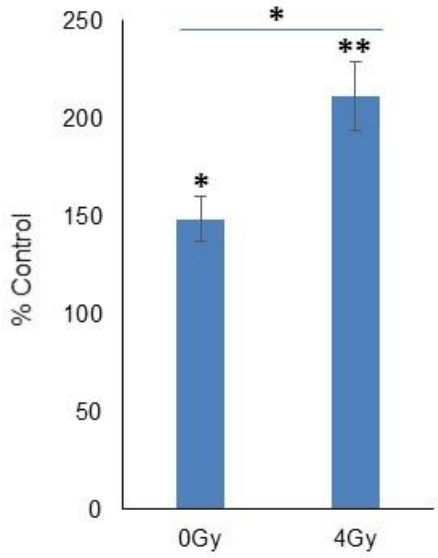

Figure 17 IBSP pre-treatment induced lasting tumor promoting functional changes.

HK157 cells were pre-treated for 7 days and assayed for proliferation 7 days post IBSP removal. The 4Gy dose of ionizing radiation was given 1 day following ligand removal. Regardless of radiation challenge, both groups were significantly more proliferative than their respective non-pre-treated control cells, and the irradiated cells displayed significantly increased cell survival than the non-irradiated cells as compared to their respective non-treated controls. *$p<0.05$, **$p<0.01$, two-tailed paired Student's t test.

Discussion

In this study we investigated a novel set of interactions between the GBM tumor cells and the tumor associated endothelial cells in the context of tumor dependence on its perivascular niche. It has been shown that GBMSCs reside in close association with the tumor microvasculature that maintains these cells in a stem-like state, (Bao et al., 2006c; Calabrese et al., 2007; Jain et al., 2007b) possibly similar to the NSC perivascular niche that regulates various stem cell properties (Louissaint et al., 2002; Palmer et al., 2000a; Ramirez-Castillejo et al., 2006; Shen et al., 2004). In order to define a core set of molecules mediating GBMSC-EC signaling, we generated a tumor-endothelial interactome, through RNA-seq whole transcriptome profiling of angiogenic GBMSCs and the associated ECs from fresh primary human GBM samples.

To obtain a differential expression signature for GBMSCs and ECs, a comparison of GBM samples to normal EC and GPC samples was necessary. This provided for an experimental limitation, as adult healthy human brain samples are usually not surgically resected, and non-transformed tissue from resections from epilepsy surgery from children and adolescents were our only available option. However, the extent to which they represent non-pathological tissue, and their developmental stage as compared to GBM samples, which have the highest incidence in older patients, may be of concern. Alternatively, post-mortem tissue could have been obtained, however, it cannot be processed in the same manner as the freshly resected GBM samples to allow for the specific cell-type isolations, and often provides low RNA integrity and yield unsuitable for RNA-seq studies. Though we did generate a PVN interactome based on GBMSC-EC DEA, which yielded a limited number of interacting groups, we were more interested

in a comprehensive view of all possible GBM-EC ligand-SC receptor interactions within the PVN, with the hypothesis that if they are present, then they may contribute to tumor-propagating downstream signaling in GBMSCs. We thus used a normalized measure of relative expression across all GBM samples, with the lenient cutoff of FPKM units>1 for at least 1/3 of the samples in order to be tolerant of GBM tumor heterogeneity, and developed a comprehensive interactome of the PVN signaling pathways. This provided for a broad view of the previously unappreciated molecular signaling systems that regulate cell-cell interactions within the tumor PVN, and included most if not all previously reported PVN EC ligand-SC receptor interactions in glioblastomas. We identified a diverse number of EC secreted growth factors, TGFβ superfamily signaling mediators, and cytokines, as expected, along with various EC secreted extracellular and basement membrane components, such as SLRPs, nidogens, and SIBLINGs with putative interactions with various GBMSC ITG receptors among other PM proteins.

The identification of functionally significant EC-produced factors is of significance in multiple ways. First, the inhibition of such factors may prevent the progression of brain tumors. Second, and possibly more importantly, such identification could lead to a fundamental understanding of what happens when brain tumor cells lose their dependence on this close relationship. This independence is highlighted by the fact that anti-angiogenic therapy invariably fails and that GBMs recur through the spread of tumor cells into the parenchyma, necessitating an uncoupling of their survival and the vascular niche (Piao et al., 2013). One mechanism for such independence could be that through their interactions within the PVN, the tumor cells transition to a more aggressive Mes phonotype, allowing for an increased proliferative and/or invasive capacity (Piao et

al., 2013). Interestingly, IPA predicted that tumor cell invasion and migration were among the most significant functions of the putative PVN interactions we identified.

Considering the vast vascular abnormalization in GBMs and their contribution to disease progression (Carmeliet and Jain, 2000; Jain et al., 2007b), the large extent of GBM-EC expression dysregulation, however, had also not been previously successfully reported, due to tissue availability limitations and probe-based expression profiling. Our experimental approach in developing the interactome, laterally allowed for identification of a core set of dysregulated genes in ECs residing the GBM PVN, encompassing previously reported signaling pathways including TGFβ and VEGF (Dieterich et al., 2012), along with various novel signaling pathways such as steroid hormone signaling, as ESR1, and pro-angiogenic inflammatory cytokine signaling of IL1A.

A concern with discovery-based approaches can be in the stratification of candidate genes. In light of the major invasive role of the PVN interactome we became interested in EC secreted RGD motif containing extracellular matrix molecules, which had the potential to interact with ITG receptors, given that ITGs have a well-established role in mediating cell movement and migration in normal tissue, and invasion in various human neoplasms (Hood and Cheresh, 2002). Among them, the IBSP angiocrine had an exclusive GBM-EC high expression pattern, and was a very highly and significantly upregulated secreted extracellular phosphoglycoprotein. Though normally found in mineralized tissue, IBSP is upregulated in various osteotropic cancers such as breast and prostate, and its high expression in high-grade gliomas correlates with poor patient survival (Xu et al., 2012), though here we report that this survival disadvantage is exclusively attributable to PN tumors.

As a SIBLING family member, IBSP contains some similar functional motifs and post-translational modifications to OPN, though SIBLINGs are not considered to be closely genetically related (Gordon et al., 2009), and may promote differential functional effects, as with the opposite expression correlation they displayed in gliomaspheres formation (Laks et al., 2016) and their differential regulation of MMPs (OPN mainly activates MMP3, where IBSP activates MMP2 (Bellahcene et al., 2008)). Furthermore, various post-translational modifications may regulate their main functions in a given environment. For example, though OPN can promote tumor cell adhesion similar to IBSP, it's been shown to do so much more robustly in its reduced phosphorylated form (Christensen et al., 2007). The spatial expression pattern of IBSP, being an exclusively vascular factor, may also confer differential function to this ligand. It may promote GBMSC cellular movement along the vascular basement membrane, in a mode of stem cell migration demonstrated in both NSCs and GBMSCs (Cuddapah et al., 2014), through mechanisms similar to IBSP-induced adhesion, homing, and metastatic migration in other tumor cells (Byzova et al., 2000).

A large body of research indicates that GBM cells exhibiting a Mesenchymal signature, display saltatory migration through interaction of focal adhesion contacts between the extracellular matrix and ITGs (Zhong et al., 2010). Furthermore, GBM cells cultured in 3D microenvironments are shown to better resemble the in vivo functional tumor phenotypes as compared to non-encapsulated cells (Pedron, 2015; Pedron et al., 2013, 2015; Pedron and Harley, 2013; Rao, 2013; Wang et al., 2014), especially in presence HA concentrations similar to that of the GBM microenvironment (Cha et al., 2016). Here, we showed a significant role in IBSP promotion of GBMSC-enriched

gliomapshere migration capacity within biomimetic 3D HA-rich hydrogel based microenvironments, mediated through the ligands' most notable interactions with ITGαV containing integrin receptors. Similar to human brain tumors, the peripheral cells displayed a migratory phonotype away from the sphere. This may be indicative of a go vs. grow phonotype where the tumor core remains a non-motile proliferative hub that can give rise to more migratory but quiescent peripheral cells. The cellular and molecular mechanisms mediating this phenomenon, however, are not well-understood and need to be further investigated and dissected, as many GBM tumor promoting factors, including OPN are both proliferation- and migration-inducing. As previously noted, glioma cells migrating along the blood vessels do exhibit some proliferative capacity (Farin et al., 2006), though the extent of which as compared to the tumor core has not been elucidated. Further studies are needed to determine whether our encapsulated migratory cells of the gliomasphere periphery do continue to display a proliferative capacity or not. In the case of IBSP, we observed a selective proliferation advantage in PN cells and only carried out the migration assays on PN gliomaspheres as categorized in (Laks et al., 2016). However, GBMSC migratory capacity of other subtypes, namely the Mesenchymal group, needs to also be further investigated, and a potential correlation between ITG expression profiles of various gliomasphere lines with their migratory potential should be explored.

In line with the increased adhesion and migration-inducing effects of IBSP, gliomaspheres treated with this angiocrine displayed a more Mes gene expression signature as compared to non-treated cells, when considering the TCGA gene sets that were used in GBM subclassifications (Verhaak et al., 2010). This Mesenchymal

transition was also accompanied by CD44 and MMP2 upregulation, along with focal adhesion kinase and integrin pathway enrichment, and activation of the Mes transition upstream regulators, NF_KB and STAT3 (Bhat et al., 2013; Carro et al., 2010). Though the Mesenchymal transition phenotype was more robust in HK157, in every case of HK217, an IBSP treated cell population moved further towards a Mesenchymal signature as compared to its control. Interestingly, in control samples, longer culture periods may have resulted in a movement towards a Mesenchymal pattern (data not shown), which would be in line with reports of environmental conditions, such as hypoxia, inducing a Mes transition (Joseph et al., 2015). However, this movement was dramatically accelerated by the treatment of the cells with the IBSP ligand.

Lastly, we demonstrated that IBSP treatment left the cells with lasting functional changes, where upon its removal, the pre-treated cells continued to display an increased proliferative capacity, and increased radioresistance, yet another hallmark of a Mes transition. This would signify an uncoupling of the GBMSC from its reliance of the IBSP angiocrine, at least temporarily. The challenge would be to determine the extent of this uncoupling in terms of time, and proportion of the cells within a culture, which would require a single-cell analysis of the IBSP effect on a given gliomasphere culture.

In conclusion, we generated a comprehensive set of specific putative interactions between GBMSCs and tumor-associated ECs within the PVN and proposed various pathways and mechanism for tumor propagation as a result of these interactions. We specifically reported on a novel and significant role for the EC-specific extracellular matrix molecule, IBSP, in promoting an invasive and aggressive phenotype at least in PN gliomasphere cultures, leading to a PN to Mes transformation of the treated cells.

The migratory action of IBSP was mediated in part through its interaction with the ITGαV integrin receptor, which is being targeted in various clinical, and pre-clinical approaches to inhibit tumor propagation. However, as with other therapeutic treatments, a lasting change towards a more aggressive phenotype may relieve the tumor cell's dependence on the targeted pathway, thus allowing for the escape of the tumor stem cells from the therapeutic measure. It is thus of great importance to further investigate the temporal and spatial dependence of tumor stem cells on microenvironmental factors such as GBM-EC ligands within the perivascular niche so as to develop better therapeutic strategies. Accordingly, considering that PN tumors often recur as as Mes GBMs (Phillips et al., 2006), inhibiting factors that promote the transition to this aggressive phenotype in the early stages of the malignant transformation may prove to be more effective than previously appreciated.

Experimental Procedures

Human Tissue Samples

Human brain tissue samples were obtained from surgical resections under approved Institutional Review Board protocols. Samples used for specific cell-type enrichment and purification were always pieces of freshly resected tissue. Un-dissociated whole samples, i.e. GBM, and GM/WM, were stored in RNAlater (Thermo Fisher Scientific) at -20ºC, or flash frozen immediately following resection, respectively. The un-dissociated samples were not used in downstream analyses, and were only included as quality check controls. Brain tumor samples were collected in collaboration with the UCLA Brain Tumor Translational Resource (BTTR), and were graded by the attending neuropathologist according to guidelines set forth by the World Health Organization (WHO). Non-transformed juvenile samples for specific cell-type isolation were collected in the operating room from 3 patients, 5-19 years old, following EEG and MRI determination of the most normal tissue areas. All tissues were collected with informed patient/guardian consent.

Tissue processing

Reagents: Percoll Plus (GE Healthcare). 11X stock buffer: 220 mM HEPES (11ml 1M Stock), 880mM NaCl (8.8ml 5M stock), 1100 mM Glycerol (11ml 50% weight/volume solution), 220 mg BSA, distilled water (19.2 ml). Working 1X Percoll solution: 10ml Percoll Plus and 1ml 11X stock buffer. 4x Buffer: 4ml 11X stock buffer and 7ml DMEM/F12.

To obtain a single cell suspension, brain samples (300-700 mg) were minced into ~1mm pieces, and incubated in 12500 U of Collagenase II (Worthington Biochemical Corp.) and 12500 U of Collagenase IV (Worthington Biochemical Corp.) in Hibernate A without Calcium and Magnesium (BrainBits, LLC) at 37ºC for 20 min with gentle agitation every 5min. Following enzymatic digestion, Dulbeco's modified Eagle's medium (DMEM)/F12 (Invitrogen) was gradually added to the partially dissociated sample, as a single cell suspension was obtained in the course of a gradual mechanical dissociation. The cell suspension was then passed through a 100µm filter and cells were pelleted at 1000xg for 5min. To remove cellular debris and red blood cells (RBC) from the sample a modified Percoll purification procedure was used. The cell pellet was re-suspended in a total volume of 1.5ml of DMEM/F12, and 1.5ml of working 1X Percoll solution. RBCs were pelleted by centrifugation of this suspension at 1000xg for 5min. To the remaining supernatant and debris 1.5ml of 4X buffer was gradually added, to facilitate a shift in osmolality that would selectively allow live cells to pellet at the next step. This mixture was then centrifuged at 3000xg for 7min, and the supernatant and debris were removed. Cells in the pellet were very gradually re-introduced to normal salt concentrations by addition of 10-15ml media, were passed through a 40µm filter, and were again pelleted by centrifugation at 1000xg for 5min. The cells were then re-suspended in 1ml of phosphate buffered saline (PBS) containing 0.1% Bovine Serum Albumin (BSA; Invitrogen), and the number of cells and their viability were assessed.

Cell-type enrichment and purification by MACS and FACS

An EC enrichment protocol was carried out using anti-human CD31 Dynabeads (ThermoFisher Scientific), according to the manufacturer's protocol for endothelial cell positive selection. From the EC-depleted fraction, A2B5+ cells were then isolated by FACS, as previously described (Auvergne et al., 2013). Briefly, cells were incubated in 500µl of A2B5 antibody supernatant (clone 105; American Type Culture Collection, Manassas, VA) for 30 minutes at 4ºC. The cells were washed in 10ml of PBS and incubated in Alexa Fluour 488 Goat anti-mouse IgM secondary antibody (1:1000 in PBS with 0.5% BSA) for 30 minutes at 4ºC. The cells were washed in 10ml of PBS, re-suspended at 1 million/ml in Hibernate A minus Phenol Red (BrainBits, LLC), supplemented with B27 (Gibco), 2µg/ml 4',6-diamidino-2-phenylindole (Dapi, Invitrogen) for dead cell exclusion, and 5µM DRAQ7 (Biotatus) for nucleated cell inclusion. Appropriate isotype controls and un-stained cells were included, and cells were sorted on a FACS ARIA flow cytometer (BD Biosciences) using the FACS DIVA software.

RNA sample preparation

Immediately following EC and A2B5+ cell preparation protocols, cells were pelleted (1000Xg, 5min), re-suspended, and lysed in 1ml QIAzol lysis reagent (QIAGEN). RNA isolation was carried out according to manufacturer's modified QIAzol protocol using the QIAGEN microRNeasy kit. Preliminary RNA concentration and quality were assessed by NanoDrop ND-1000 spectrophotometer (NanoDrop Technologies).

RNA Sequencing

Total RNA integrity was examined using the Agilent Bioanalyzer 2000 (Agilent, Santa Clara, CA) and quantified with NanoDrop® (Thermo-Fischer, Waltham, MA). Four point eight nanograms of total RNA were used to generate cDNA using Ovation® RNA-Seq System V2 (NuGEN, San Carlos, CA) following the manufacturer's instruction. One hundred nanograms of cDNA were used in the library preparation using Ovation® Ultralow Library Systems (NuGEN). The cDNA was fragmented to 300 bp using the Covaris M220 (Covaris, Woburn, MA) then followed the manufacturer's instruction for end repair, adaptor ligation and library amplification. All samples were multiplexed into a single pool in order to avoid batch effects and sequenced using an Illumina HiSeq 2000 sequencer (Illumina, San Diego, CA) in high output mode across 9 lanes of 50bp-paired-end sequencing, corresponding to 4.3 samples per lane and yielding between ~45 million reads per sample. Quality control was performed on base qualities and nucleotide composition of sequences. Alignment to the H.sapiens (Hg38) refSeq (refFlat) reference gene annotation was performed using the STAR spliced read aligner with default parameters. Additional QC was performed after the alignment to examine: the level of mismatch rate, mapping rate to the whole genome, repeats, chromosomes, key transcriptomic regions (exons, introns, UTRs, genes), insert sizes, AT/GC dropout, transcript coverage and GC bias. Outliers were removed based on QC results. Between 60 and 82% (avg 76%) of the reads mapped uniquely to the human genome. Total counts of read-fragments aligned to candidate gene regions were derived using HTSeq program (www.huber.embl.de/users/anders/HTSeq/doc/overview.html) with Human Hg38 (Dec.2014) refSeq (refFlat table) as a reference and used as a basis for the

quantification of gene expression. Only uniquely mapped reads were used for subsequent analyses. Differential expression analysis was conducted with R-project and the Bioconductor package edgeR. Statistical significance of the differential expression, expressed as Log_2 Fold Change (logFC), was determined, using tag-wise dispersion estimation, at p-Value of <0.005 unless stated otherwise. FPKM values were reported as measure of relative expression units.

Ingenuity pathway analysis software

IPA (www.ingenuity.com; QIAGEN) was used in determining cellular localization of GBMSC/EC genes, and identifying direct and indirect protein interactions among EC extracellular factors and GBMSC PM molecules, along with manual curation and minimal use of the STRING functional protein association networks online tool (http://string-db.org), which was instrumental in developing both interactomes (according to DEA, and the comprehensive interactome according to FPKM expression units). Canonical pathways, upstream regulators and disease and functions associated with a gene list were considered to be significant at p<0.05 unless state otherwise.

Immunohistochemistry (IHC) and immunofluorescence (IF)

Formalin fixed paraffin embedded (FFPE) patient GBM tissue blocks were sectioned at a thickness of 10µm. Sections were deparaffinized by passing the slides through 2 changes of xylene (5mins each), followed by 100%, 95%, 70%, 50%, and 30% ethanol, and deionized water (2mins each) to allow for their rehydration. Standard citrate buffer (0.1M sodium citrate pH 6.1) -mediated antigen retrieval (95ºC for 10mins),

and pepsin-mediated antigen retrieval (37ºC for 10mins) were carried out. All washes were done in Tris buffered saline (TBS) or TBS with 0.1% Tween20 (TBST).

For IHC, the sections' endogenous peroxidase activity was quenched in 0.3% H_2O_2 in TBS for 10 mins, followed by 3, 2 minute washes in TBST. Sections were incubated in blocking solution (5% Normal Goat or Donkey serum and 1% BSA in TBST) for 30 minutes. They were then incubated with the primary antibody, IBSP (LFMb-25, Santa Cruz Biotechnology, INC., 1:20) overnight at 4ºC in a humidified chamber. Sections were washed 3 times with TBST (5 mins each), and incubated in the appropriate biotinylated secondary antibody for 45 mins at room temperature. Vectastain Elite ABC HRP kit and Vector DAB kit (PK6100, and SK4100, Vector Laboratories) were then used according to manufacturer's protocol. Following hematoxylin nuclear counter staining (2min), sections were washed in an excess of deionized water, and dehydrated by passing them through 100%, 95%, 70%, 50%, 30% ethanol (2 mins each). They were passed through two changes of xylene (2 mins each) and allowed to air dry before mounting by Permount (Fisher).

For IF, sections were permeablized in TBS plus 0.1% TritonX100, washed 2 more times, 5 mins each with TBST, and incubated in blocking solution (5% Normal Goat or Donkey serum and 1% BSA in TBST) for 30 minutes. They were then incubated in primary antibodies, IBSP (LFMb-25, Santa Cruz Biotechnology, INC., 1:20), VWF (Ab6994, Abcam, 1:200) diluted in blocking solution, overnight at 4ºC in a humidified chamber. Sections were washed 3 times with TBST (5 mins each), and incubated in the appropriate secondary antibody (Alexa Fluor, ThermoFisher Scientific, 1:1000) for 2 hours at room temperature. Sections were washed in TBST with Hoechst nuclear

counter stain for 5 minutes, followed by 2 more washes with TBST (5 mins each). Sections were mounted by FluoroGel (Gene Tex), and sealed with nail polish.

Gliomasphere cultures

GBM-derived primary human cultures were previously described (Hemmati et al., 2003; Laks et al., 2009). Gliomaspheres were cultures in DMEM/F12 supplemented with B27 (Gibco), 20 ng/ml basic fibroblast growth factor (bFGF, Peprotech), 50ng/ml epidermal growth factor (EGF, Life Technologies), penicillin/streptomycin (Invitrogen), Glutamax (Invitrogen), and 5ug/ml heparin (Sigma-Aldrich). Gliomasphers were dissociated down to single cells with Accumax (Sigma) every 7-14 days depending on growth rate.

Synthesis and characterization of thiolated hyaluronic acid used in hydrogels

Sodium hyaluronate (700kDa, LifeCore) was dissolved in deionized water (10 mg/mL). 1-Ethyl-3-[3-dimethylaminopropyl]carbodiimide (EDC, Thermo Scientific Pierce) dissolved in deionized water, was added to the HA solution at a molar ratio of 4:1 (EDC:HA carboxyls), unless otherwise stated. N-hydroxysuccinimide (NHS, Acros Organics) was then added at a molar ratio of 1:2 (NHS:EDC) in all cases. The pH was adjusted to 5.5 with 0.1M HCl. The pH was then readjusted to 5.5. The solution was stirred at room temperature for 45 minutes before adding cystamine dihydrochloride (Sigma-Aldrich) at a molar ratio of 4:1 (cystamine:HA carboxyls). The pH was adjusted to 6.25 with 0.1M NaOH and the reaction solution stirred at room temperature overnight.

Addition of dithiothreitol (DTT, Sigma-Aldrich) (pH 8) was added in molar excess (4x) to cystamine and incubated for 2 hours to cleave cystamine disulfides. The reaction was quenched by adjusting the pH to 4 and the solution dialyzed against 2L of acidic (pH 4) deionized water for 3 days. Purified, thiolated HA (HA-SH) was filtered through a 0.22μm filter (EMD Millipore), frozen, lyophilized until dry, and stored with desiccant at -20°C until use. HA thiolation was confirmed using proton NMR spectroscopy and an Ellman's test for free thiols (Bernkop-Schnurch et al., 1999).

Hydrogel formation and encapsulation of GBM spheroids

4-arm polyethylene glycol-vinyl sulfone (PEG-VS, 20kDa, Laysan Bio) was dissolved in PBS 10 mM (pH 7.4) at 50 mg/mL. Peptides were conjugated to PEG-VS via N-terminal cysteine groups. Peptide (2mM stock in PBS) was added to the PEG-VS solution to achieve a solution of 250μM peptide and 20 mg/mL PEG-VS. The reaction was allowed to proceed at 37 ˚C for 2 hours. Lyophilized, thiolated HA was dissolved in 20mM HEPES (pH 10) at 20 mg/mL and pH adjusted to 7 with 1M NaOH after dissolution. Thiolated HA and peptide-conjugated PEG-VS were mixed in equal volumes immediately before injection into culture wells. Gelation was allowed to proceed for 90 min. at 37 ˚C. At 90 min., isolated GBM spheroids were injected into the partially crosslinked hydrogels. Hydrogels with embedded spheroids were then crosslinked to completion (30 min. incubation at 37˚C) before addition of cell culture medium.

Imaging migration (small-scale)

Hydrogels were imaged periodically using wide-field fluorescence microscopy (Zeiss Axiovert observer.Z1). At the end of the experiment period, confocal images were acquired (Leica SP5).

Migration quantification (small-scale)

At each time point, images were analyzed using Image J software (NIH). Migration was quantified by measuring the furthest distance cells migrated from the peripheral edge of each GBM spheroid. For each condition 15 spheroids from 5 separate hydrogels were subjected to the measurement unless state otherwise. Data are shown as the average migration distance for each condition ± standard error of the mean (SEM).

High-throughput imaging and quantification of gliomasphere migration

In order to utilize interfering RNA technologies, we developed a high-throughput (HT) method to assess cellular dispersion in our 3D microenvironments. We encapsulated gliomaspheres in hydrogels plated in 384-well Greiner plates, which were imaged using a Molecular Devices ImageXpress XL platform. In short, plates were imaged using a Nikon 10x objective (0.3NA, Plan Apo) with no binning and laser auto-focusing. Plates were imaged daily, and were treated with Hoechst, at 1:3000 in media, overnight before the final imaging that were to be used for quantification. The resulting images were analyzed using the MetaXpress Custom Module editor. A custom module was set up using Adaptive Tresholding in the UV/DAPI channel with a size window from 10-400m micron and an intensity over local background of at least 1750 grey scales.

This analysis applied a mask to the images, thus allowing for quantification of the number of objects dispersed within the hydrogel. Though this method of quantification is an underestimation of the number of cells, it does provide for an efficient means to quantify dispersion from the gliomasphere core for our HT purposes. The following parameters were extracted on an object by object base: Total area average, area average per object, centroid position for x and y axis. Also, the sums for the same parameters were extracted. The Elledge form factor was extracted on an object by object base.

shRNA Screening

shRNA clones of the genes of interest were arrayed from our genome wide shRNA library (Silva et al., 2005) and grown up in LB using standard molecular biology methods. In a next step, plasmid DNA was prepared using Macherey and Nagel Nucleobond kits according to the manufacturer's recommendations. Virus was produced as previously reported: Briefly, 100 ng shRNA encoding pGIPZ plasmid was spotted into PDL coated 96 well plates and 100 ng pCMVd8.91 with 10 ngpMD2G was added together with Mirus TransIT in a 1:3 ratio and incubated for 20 min in a total volume of 25 µL. 75 µL containing 40,000 293T cells were added on top to a total of 100 µL in DMEM with 30% FBS with 1x PSG, NEN and HEPES. Successful transfection was confirmed after 24 hours at 37°C and 5% CO_2 by GFP expression of the cells. Plates were washed twice with PBS and the supernatant replaced with DMEM/F12 supplemented with B27. Virus was harvested after another 48 hours at 37°C and 5% CO_2 and 7.5 µL virus containing media was plated into each well of a 384 well plate

using an Agilent Vprep in a custom HEPA filtered enclosure. Media was added to 25µL total volume before cells were added at [100000/ml], to a total of 50ul volume/well. Three days post transduction, small GBM spheroids were encapsulated in hydrogels plated in another 384-well plate.

Cell Proliferation Assay

The Dojindo Cell Counting Kit-8 (Dojindo Molecular Technologies Inc.) was used according to the manufacturer's protocol. Freshly dissociated gliomaspheres were plated at 5000cells/100µl/well in a 97-well plate and allowed to proliferated for 7 days at which point cell numbers of the experimental conditions (250nM IBSP in all cases unless specified otherwise) were assessed as compared to control (CTRL) conditions.

Microarray-based gene expression analysis

Concentration and quality of RNA samples were examined using the NanoDrop ND-1000 Spectrophotometer (NanoDrop Technologies) and the Agilent 2100 Bioanalyzer (Agilent Technologies). RNA samples were reverse transcribed and labeled according to the manufacturer's instructions and hybridized to Affymetrix high-density oligonucleotide HG-U133A Plus 2.0 Human Arrays. Microarray data analysis was performed as described previously (21913117). Briefly, array preprocessing was completed in the R computing environment (http://www.r-project. org) using Bioconductor packages (http://www.bioconductor.org). Raw data were normalized using the robust multiarray method (12582260). To eliminate batch effects, additional normalization was performed using the R package "ComBat"

(http://statistics.byu.edu/johnson/ComBat; 16632515) with default parameters. Contrast analysis of differential expression was performed using the LIMMA package (Smyth 2005, Smyth, G. K. 2005. “Limma: Linear Models for Microarray Data.” In Bioinformatics and Computational Biology Solutions Using R and Bioconductor, edited by R. Gentleman, V. Carey, S. Dudoit, R. Irizarry, and W. Huber, 397–420. Springer, New York). After linear model fitting, a Bayesian estimate of differential expression was calculated using a modified t test. The threshold for statistical significance was set at $P < 0.005$ for differential expression analysis and $P < 0.01$ for explorative analyses (gene ontology and pathway analysis). Gene ontology and pathway analysis were carried out using the Database for Annotation, Visualization and Integrated Discovery (DAVID, https://david.ncifcrf.gov), GSEA (16199517), and Ingenuity Pathway Analysis (IPA; www.ingenuity.com).

TCGA gliomasphere classification

Our gliomasphere transcriptomes were classified into the three (Classical, Mes, and PN) clinically relevant TCGA subclassifications as previous described (Laks et al., 2016). Briefly, the 173 core TCGA glioblastoma samples used in TCGA subclassifications of GBMs (Verhaak et al., 2010) were used to build our classification model. The TCGA unified gene expression data (across three microarray platforms: Affymetrix HuEx array, Affymetrix U133A array and Agilent 244K) were combined with our gliomasphere data from Affymetrix U133 plus 2.0 array, and utilizing the limma R package, they were normalized together (Smyth, 2005). Following batch effect normalization using the ComBat R package (http://statistics.byu.edu/johnson/ComBat/)

(Johnson et al., 2007), we used the LDA based centroid classification algorism (ClaNC) used by (Verhaak et al., 2010), to develop a 3-class centroid-based classifier from 38 Classical, 56 Mes, and 53 PN TCGA samples (Dabney, 2006), where the 26 TCGA neural samples were excluded. Only 789 of the of the 840 TCGA classifier genes were used to assign classifications to our gliomaspheres, due to limitations in gene name overlap between TCGA and our platforms.

Statistics

Small group comparisons were carried out in Excel using the Student's t test, where significance was determined at $p<0.05$ unless state otherwise. All figure error bars shown are a measure of the Standard Error of Mean (SEM) unless specified otherwise. Gene expression and correlation statistical analysis methods were describe above.

Chapter 5

Summary and Perspectives

Novel therapeutic avenues in treating GBMs will have to combine targeting molecules important at various stages of cancer progression. Thus targeting the niche that promotes the invasion, malignant progression, and in effect the recurrence of the tumor may provide for an effective therapeutic avenue. The endothelial cells of the extensive GBM tumor neovasculature and the GBMSCs in close association with them have a bi-directional regulatory relationship. Though the GBMSC regulation of ECs have been extensively studied, a limited amount of investigation into EC maintenance of GBMSC stem-like characteristics had previously been reported on.

Here, we explored the putative interactions between tumor endothelial extracellular molecules and GBMSC plasma membrane molecules in order to elucidate the signaling pathways underlying tumor dependence on its perivascular niche. Our putative interactome, based on FPKM relative gene expression units, provided the most comprehensive view of the complexity of this dependence to date. Our data has the potential to fuel not only studies at the molecular level on single interaction units, but it also may provide the opportunity for generation of models that simulate the co-existence of all these pathways within a GBMSC protective niche. The relative expression of molecules, and all previously published data can be used to assign the nodes, connections, and the weight for the various interactions, and dominant signaling pathways may be identified in a manner that may unclutter and unify the vast amount of molecular data we are reporting on, in PVN regulation of GBMSCs.

Though we did not have the resources to undertake such a large-scale computational analysis of our GBM perivascular niche interactome, we did attempt to identify a major role for the GBMSC-EC interactions through gene ontology analyses. We thus showed that cellular movement and increased migratory capacity were among the most significant functions of the PVN signaling pathways. We then moved to validate a target that contributed to this significant function and chose the secreted, soluble, RGD motif-containing Integrin Binding Sialoprotein (IBSP) for downstream functional studies. We showed that IBSP promoted gliomasphere migration in 3D HA-rich hydrogel based microenvironments. To next identify the GBMSC receptors that mediated the IBSP migratory action, we developed a novel high-throughput platform for *in vitro* assessment of tumor invasion within the biomimetic 3D microenvironments. This platform may later be utilized in combination with various currently-available therapeutics, libraries of small-molecule regulators, and/or shRNA libraries to allow for targeted and/or discovery-based studies into pathways and treatments of GBM invasion. In our studies, we used our screening methodology to demonstrate that ITGαV played a significant role in mediating IBSP induction of invasion in gliomasphere lines.

IBSP-induced gliomasphere migration consisted of peripheral sphere cells invading into the hydrogel matrix and away from the sphere core. In human neoplasms a similar phenomenon is observed in that the proliferative tumor core gives rise to migratory peripheral cells, though it is unclear how quiescent the migratory cells are. Little is known regarding this putative dichotomy of proliferation vs. migration. Migrating NSCs continue to divide through their path along blood vessels scaffolds and a study has shown this to be true of migrating glioma cells as well in orthotopic

xenotransplantation models (Farin et al., 2006). Thus it is unclear whether such a dichotomy really does exist. In our model, we could assess the proliferative capacity of the migrating cells as compared to the sphere mass in order to further investigate this topic.

Interestingly, GBM expression of IBSP only correlated with poor prognosis in PN tumors in both the TCGA and Rembrandt GBM databases (2008; Madhavan et al., 2009), and IBSP exclusively promoted PN gliomasphere proliferation, though we did not explore its migratory action in any subtype other than PN. Thus the invasive function of IBSP in other GBM subtypes needs to be further investigated. Since IBSP differentially regulated GBM subtypes in proliferation, and induced an invasive phenotype, we next investigated its contribution to promoting more aggressive tumor cells. Our studies revealed that IBSP induced a Mesenchymal transition in gliomasphere expression signature, which was accompanied by activation of Mes regulators, NF_KB, and STAT3, and upregulation of MM2 and the CD44 Mes marker.

Though EC secreted factors promote tumor initiation, growth, and cell survival (Calabrese et al., 2007), and GBMSCs seek out, migrate, and proliferate along the blood vessels (Farin et al., 2006; Watkins et al., 2014), the temporal and spatial extent of the GBMSC dependence on the vasculature remains unknown. Our *in vitro* studies demonstrated that IBSP pre-treatment promoted a lasting functional effect on gliomasphere proliferation, and increased radio-resistance in the absence of ligand. This may signify a potential first step in the fundamental understanding of what happens when GBM cells lose their dependence on the perivascular niche, in that they may

assume a lasting, more aggressive, and invasive phenotype through their interactions with vascular factors such as IBSP. It is important to note that the exact association of IBSP with GBM-ECs and the mode of invasion induced by it, along vessels or diffuse, must be investigated further in *in vivo* GBM models. Additionally, the number of cells that are spatially exposed to high enough IBSP concentrations that would induce such lasting changes, what those concentrations may be *in vivo*, the permanency of such changes, and any potential lasting GBMSC migratory effects, remain as topics for further investigated.

References

(2008). Comprehensive genomic characterization defines human glioblastoma genes and core pathways. Nature *455*, 1061-1068.

Alcantara Llaguno, S., Chen, J., Kwon, C.H., Jackson, E.L., Li, Y., Burns, D.K., Alvarez-Buylla, A., and Parada, L.F. (2009). Malignant astrocytomas originate from neural stem/progenitor cells in a somatic tumor suppressor mouse model. Cancer cell *15*, 45-56.

Anderson, J.C., McFarland, B.C., and Gladson, C.L. (2008). New molecular targets in angiogenic vessels of glioblastoma tumours. Expert reviews in molecular medicine *10*, e23.

Assanah, M., Lochhead, R., Ogden, A., Bruce, J., Goldman, J., and Canoll, P. (2006). Glial progenitors in adult white matter are driven to form malignant gliomas by platelet-derived growth factor-expressing retroviruses. The Journal of neuroscience : the official journal of the Society for Neuroscience *26*, 6781-6790.

Auvergne, R.M., Sim, F.J., Wang, S., Chandler-Militello, D., Burch, J., Al Fanek, Y., Davis, D., Benraiss, A., Walter, K., Achanta, P.*, et al.* (2013). Transcriptional Differences between Normal and Glioma-Derived Glial Progenitor Cells Identify a Core Set of Dysregulated Genes. Cell reports *3*, 2127-2141.

Bao, S., Wu, Q., McLendon, R.E., Hao, Y., Shi, Q., Hjelmeland, A.B., Dewhirst, M.W., Bigner, D.D., and Rich, J.N. (2006a). Glioma stem cells promote radioresistance by preferential activation of the DNA damage response. Nature *444*, 756-760.

Bao, S., Wu, Q., McLendon, R.E., Hao, Y., Shi, Q., Hjelmeland, A.B., Dewhirst, M.W., Bigner, D.D., and Rich, J.N. (2006b). Glioma stem cells promote radioresistance by preferential activation of the DNA damage response. Nature *444*, 756-760.

Bao, S., Wu, Q., Sathornsumetee, S., Hao, Y., Li, Z., Hjelmeland, A.B., Shi, Q., McLendon, R.E., Bigner, D.D., and Rich, J.N. (2006c). Stem cell-like glioma cells promote tumor angiogenesis through vascular endothelial growth factor. Cancer research *66*, 7843-7848.

Bellahcene, A., Castronovo, V., Ogbureke, K.U., Fisher, L.W., and Fedarko, N.S. (2008). Small integrin-binding ligand N-linked glycoproteins (SIBLINGs): multifunctional proteins in cancer. Nature reviews Cancer *8*, 212-226.

Bernkop-Schnurch, A., Schwarz, V., and Steininger, S. (1999). Polymers with thiol groups: A new generation of mucoadhesive polymers? Pharmaceut Res *16*, 876-881.

Bhat, K.P., Balasubramaniyan, V., Vaillant, B., Ezhilarasan, R., Hummelink, K., Hollingsworth, F., Wani, K., Heathcock, L., James, J.D., Goodman, L.D.*, et al.* (2013). Mesenchymal differentiation mediated by NF-kappaB promotes radiation resistance in glioblastoma. Cancer cell *24*, 331-346.

Bondy, M.L., Scheurer, M.E., Malmer, B., Barnholtz-Sloan, J.S., Davis, F.G., Il'yasova, D., Kruchko, C., McCarthy, B.J., Rajaraman, P., Schwartzbaum, J.A.*, et al.* (2008). Brain tumor epidemiology: consensus from the Brain Tumor Epidemiology Consortium. Cancer *113*, 1953-1968.

Borovski, T., Beke, P., van Tellingen, O., Rodermond, H.M., Verhoeff, J.J., Lascano, V., Daalhuisen, J.B., Medema, J.P., and Sprick, M.R. (2013). Therapy-resistant tumor microvascular endothelial cells contribute to treatment failure in glioblastoma multiforme. Oncogene *32*, 1539-1548.

Bozoyan, L., Khlghatyan, J., and Saghatelyan, A. (2012). Astrocytes Control the Development of the Migration-Promoting Vasculature Scaffold in the Postnatal Brain via VEGF Signaling. Journal of Neuroscience *32*, 1687-1704.

Brem, S., Cotran, R., and Folkman, J. (1972). Tumor angiogenesis: a quantitative method for histologic grading. Journal of the National Cancer Institute *48*, 347-356.

Byzova, T.V., Kim, W., Midura, R.J., and Plow, E.F. (2000). Activation of integrin alpha(V)beta(3) regulates cell adhesion and migration to bone sialoprotein. Exp Cell Res *254*, 299-308.

Calabrese, C., Poppleton, H., Kocak, M., Hogg, T.L., Fuller, C., Hamner, B., Oh, E.Y., Gaber, M.W., Finklestein, D., Allen, M.*, et al.* (2007). A perivascular niche for brain tumor stem cells. Cancer cell *11*, 69-82.

Carmeliet, P., and Jain, R.K. (2000). Angiogenesis in cancer and other diseases. Nature *407*, 249-257.

Carro, M.S., Lim, W.K., Alvarez, M.J., Bollo, R.J., Zhao, X., Snyder, E.Y., Sulman, E.P., Anne, S.L., Doetsch, F., Colman, H.*, et al.* (2010). The transcriptional network for mesenchymal transformation of brain tumours. Nature *463*, 318-325.

Cha, J., Kang, S.-G., and Kim, P. (2016). Strategies of Mesenchymal Invasion of Patient-derived Brain Tumors: Microenvironmental Adaptation. Scientific Reports *6*, 24912.

Charles, N., and Holland, E.C. (2010). The perivascular niche microenvironment in brain tumor progression. Cell cycle *9*, 3012-3021.

Charles, N., Ozawa, T., Squatrito, M., Bleau, A.-M., Brennan, C.W., Hambardzumyan, D., and Holland, E.C. Perivascular Nitric Oxide Activates Notch Signaling and Promotes Stem-like Character in PDGF-Induced Glioma Cells. Cell stem cell *6*, 141-152.

Cheng, L., Huang, Z., Zhou, W., Wu, Q., Donnola, S., Liu, J.K., Fang, X., Sloan, A.E., Mao, Y., Lathia, J.D.*, et al.* (2013). Glioblastoma stem cells generate vascular pericytes to support vessel function and tumor growth. Cell *153*, 139-152.

Christensen, B., Kazanecki, C.C., Petersen, T.E., Rittling, S.R., Denhardt, D.T., and Sorensen, E.S. (2007). Cell type-specific post-translational modifications of mouse

osteopontin are associated with different adhesive properties. The Journal of biological chemistry *282*, 19463-19472.

Colman, H., Zhang, L., Sulman, E.P., McDonald, J.M., Shooshtari, N.L., Rivera, A., Popoff, S., Nutt, C.L., Louis, D.N., Cairncross, J.G.*, et al.* (2010). A multigene predictor of outcome in glioblastoma. Neuro-oncology *12*, 49-57.

Cooper, L.A., Gutman, D.A., Long, Q., Johnson, B.A., Cholleti, S.R., Kurc, T., Saltz, J.H., Brat, D.J., and Moreno, C.S. (2010). The proneural molecular signature is enriched in oligodendrogliomas and predicts improved survival among diffuse gliomas. PloS one *5*, e12548.

Cuddapah, V.A., Robel, S., Watkins, S., and Sontheimer, H. (2014). A neurocentric perspective on glioma invasion. Nature reviews Neuroscience *15*, 455-465.

Dabney, A.R. (2006). ClaNC: point-and-click software for classifying microarrays to nearest centroids. Bioinformatics *22*, 122-123.

Dieterich, L.C., Mellberg, S., Langenkamp, E., Zhang, L., Zieba, A., Salomaki, H., Teichert, M., Huang, H., Edqvist, P.H., Kraus, T.*, et al.* (2012). Transcriptional profiling of human glioblastoma vessels indicates a key role of VEGF-A and TGFbeta2 in vascular abnormalization. The Journal of pathology *228*, 378-390.

Dolecek, T.A., Propp, J.M., Stroup, N.E., and Kruchko, C. (2012). CBTRUS statistical report: primary brain and central nervous system tumors diagnosed in the United States in 2005-2009. Neuro-oncology *14 Suppl 5*, v1-49.

Farin, A., Suzuki, S.O., Weiker, M., Goldman, J.E., Bruce, J.N., and Canoll, P. (2006). Transplanted glioma cells migrate and proliferate on host brain vasculature: a dynamic analysis. Glia *53*, 799-808.

Fillmore, H.L., VanMeter, T.E., and Broaddus, W.C. (2001). Membrane-type Matrix Metalloproteinases (MT-MMP)s: Expression and Function During Glioma Invasion. J Neuro-Oncol *53*, 187-202.

Fisher, J.L., Schwartzbaum, J.A., Wrensch, M., and Wiemels, J.L. (2007). Epidemiology of brain tumors. Neurologic clinics *25*, 867-890, vii.

Fuchs, E., Tumbar, T., and Guasch, G. (2004). Socializing with the neighbors: Stem cells and their niche. Cell *116*, 769-778.

Galli, R., Binda, E., Orfanelli, U., Cipelletti, B., Gritti, A., De Vitis, S., Fiocco, R., Foroni, C., Dimeco, F., and Vescovi, A. (2004). Isolation and characterization of tumorigenic, stem-like neural precursors from human glioblastoma. Cancer research *64*, 7011-7021.

Gordon, J.A.R., Sodek, J., Hunter, G.K., and Goldberg, H.A. (2009). Bone sialoprotein stimulates focal adhesion-related signaling pathways: Role in migration and survival of breast and prostate cancer cells. Journal of Cellular Biochemistry *107*, 1118-1128.

Hegi, M.E., Diserens, A.C., Gorlia, T., Hamou, M.F., de Tribolet, N., Weller, M., Kros, J.M., Hainfellner, J.A., Mason, W., Mariani, L.*, et al.* (2005). MGMT gene silencing and benefit from temozolomide in glioblastoma. The New England journal of medicine *352*, 997-1003.

Hemmati, H.D., Nakano, I., Lazareff, J.A., Masterman-Smith, M., Geschwind, D.H., Bronner-Fraser, M., and Kornblum, H.I. (2003). Cancerous stem cells can arise from pediatric brain tumors. Proceedings of the National Academy of Sciences of the United States of America *100*, 15178-15183.

Hood, J.D., and Cheresh, D.A. (2002). Role of integrins in cell invasion and migration. Nature reviews Cancer *2*, 91-100.

Huse, J.T., Phillips, H.S., and Brennan, C.W. (2011). Molecular subclassification of diffuse gliomas: seeing order in the chaos. Glia *59*, 1190-1199.

Hwang, Q., Cheifetz, S., Overall, C.M., McCulloch, C.A., and Sodek, J. (2009). Bone sialoprotein does not interact with pro-gelatinase A (MMP-2) or mediate MMP-2 activation. BMC cancer *9*, 121.

Iadecola, C., and Nedergaard, M. (2007). Glial regulation of the cerebral microvasculature. Nature neuroscience *10*, 1369-1376.

Ignatova, Z., Hornle, C., Nurk, A., and Kasche, V. (2002). Unusual signal peptide directs penicillin amidase from Escherichia coli to the Tat translocation machinery. Biochemical and biophysical research communications *291*, 146-149.

Jackson, E.L., Garcia-Verdugo, J.M., Gil-Perotin, S., Roy, M., Quinones-Hinojosa, A., VandenBerg, S., and Alvarez-Buylla, A. (2006). PDGFR alpha-positive B cells are neural stem cells in the adult SVZ that form glioma-like growths in response to increased PDGF signaling. Neuron *51*, 187-199.

Jadin, L., Pastorino, S., Symons, R., Nomura, N., Jiang, P., Juarez, T., Makale, M., and Kesari, S. (2015). Hyaluronan expression in primary and secondary brain tumors. Annals of Translational Medicine *3*.

Jain, R.K., di Tomaso, E., Duda, D.G., Loeffler, J.S., Sorensen, A.G., and Batchelor, T.T. (2007a). Angiogenesis in brain tumours. Nature reviews Neuroscience *8*, 610-622.

Jain, R.K., di Tomaso, E., Duda, D.G., Loeffler, J.S., Sorensen, A.G., and Batchelor, T.T. (2007b). Angiogenesis in brain tumours. Nature reviews Neuroscience *8*, 610-622.

Jeon, H.M., Kim, S.H., Jin, X., Park, J.B., Kim, S.H., Joshi, K., Nakano, I., and Kim, H. (2014). Crosstalk between glioma-initiating cells and endothelial cells drives tumor progression. Cancer research *74*, 4482-4492.

Jhaveri, N., Chen, T.C., and Hofman, F.M. (2014). Tumor vasculature and glioma stem cells: Contributions to glioma progression. Cancer letters.

Johnson, W.E., Li, C., and Rabinovic, A. (2007). Adjusting batch effects in microarray expression data using empirical Bayes methods. Biostatistics *8*, 118-127.

Joseph, J.V., Conroy, S., Pavlov, K., Sontakke, P., Tomar, T., Eggens-Meijer, E., Balasubramaniyan, V., Wagemakers, M., den Dunnen, W.F.A., and Kruyt, F.A.E. (2015). Hypoxia enhances migration and invasion in glioblastoma by promoting a mesenchymal shift mediated by the HIF1 alpha-ZEB1 axis. Cancer letters *359*, 107-116.

Kaisorn L. Chaichana, Matthew J. McGirt, John Laterra, Alessandro Olivi, and Alfredo Quiñones-Hinojosa (2010). Recurrence and malignant degeneration after resection of adult hemispheric low-grade gliomas. Journal of Neurosurgery *112*, 10-17.

Krishnan, S., Szabo, E., Burghardt, I., Frei, K., Tabatabai, G., and Weller, M. (2015). Modulation of cerebral endothelial cell function by TGF-beta in glioblastoma: VEGF-dependent angiogenesis versus endothelial mesenchymal transition. Oncotarget *6*, 22480-22495.

Laks, D.R., Crisman, T.J., Shih, M.Y., Mottahedeh, J., Gao, F., Sperry, J., Garrett, M.C., Yong, W.H., Cloughesy, T.F., Liau, L.M.*, et al.* (2016). Large-scale assessment of the gliomasphere model system. Neuro-oncology.

Laks, D.R., Masterman-Smith, M., Visnyei, K., Angenieux, B., Orozco, N.M., Foran, I., Yong, W.H., Vinters, H.V., Liau, L.M., Lazareff, J.A.*, et al.* (2009). Neurosphere Formation Is an Independent Predictor of Clinical Outcome in Malignant Glioma. Stem Cells *27*, 980-987.

Lamour, V., Henry, A., Kroonen, J., Nokin, M.J., von Marschall, Z., Fisher, L.W., Chau, T.L., Chariot, A., Sanson, M., Delattre, J.Y.*, et al.* (2015). Targeting osteopontin suppresses glioblastoma stem-like cell character and tumorigenicity in vivo. Int J Cancer *137*, 1047-1057.

Lathia, J.D., Gallagher, J., Heddleston, J.M., Wang, J., Eyler, C.E., Macswords, J., Wu, Q., Vasanji, A., McLendon, R.E., Hjelmeland, A.B.*, et al.* (2010). Integrin alpha 6 regulates glioblastoma stem cells. Cell stem cell *6*, 421-432.

Lathia, J.D., Mack, S.C., Mulkearns-Hubert, E.E., Valentim, C.L., and Rich, J.N. (2015). Cancer stem cells in glioblastoma. Genes & development *29*, 1203-1217.

Lewis, C.E., and Pollard, J.W. (2006). Distinct role of macrophages in different tumor microenvironments. Cancer research *66*, 605-612.

Liu, C., Sage, J.C., Miller, M.R., Verhaak, R.G., Hippenmeyer, S., Vogel, H., Foreman, O., Bronson, R.T., Nishiyama, A., Luo, L.*, et al.* (2011). Mosaic analysis with double markers reveals tumor cell of origin in glioma. Cell *146*, 209-221.

Louis, D.N., Ohgaki, H., Wiestler, O.D., Cavenee, W.K., Burger, P.C., Jouvet, A., Scheithauer, B.W., and Kleihues, P. (2007). The 2007 WHO classification of tumours of the central nervous system. Acta Neuropathol *114*, 97-109.

Louissaint, A., Jr., Rao, S., Leventhal, C., and Goldman, S.A. (2002). Coordinated interaction of neurogenesis and angiogenesis in the adult songbird brain. Neuron *34*, 945-960.

Madhavan, S., Zenklusen, J.-C., Kotliarov, Y., Sahni, H., Fine, H.A., and Buetow, K. (2009). Rembrandt: Helping Personalized Medicine Become a Reality through Integrative Translational Research. Molecular Cancer Research *7*, 157-167.

Mathiisen, T.M., Lehre, K.P., Danbolt, N.C., and Ottersen, O.P. (2010). The Perivascular Astroglial Sheath Provides a Complete Covering of the Brain Microvessels: An Electron Microscopic 3D Reconstruction. Glia *58*, 1094-1103.

Miletic, H., Niclou, S.P., Johansson, M., and Bjerkvig, R. (2009). Anti-VEGF therapies for malignant glioma: treatment effects and escape mechanisms. Expert opinion on therapeutic targets *13*, 455-468.

Montana, V., and Sontheimer, H. (2011). Bradykinin promotes the chemotactic invasion of primary brain tumors. The Journal of neuroscience : the official journal of the Society for Neuroscience *31*, 4858-4867.

Moore, K.A., and Lemischka, I.R. (2006). Stem cells and their niches. Science *311*, 1880-1885.

Murakami, Y., Watari, K., Shibata, T., Uba, M., Ureshino, H., Kawahara, A., Abe, H., Izumi, H., Mukaida, N., Kuwano, M.*, et al.* (2013). N-myc downstream-regulated gene 1 promotes tumor inflammatory angiogenesis through JNK activation and autocrine loop of interleukin-1alpha by human gastric cancer cells. The Journal of biological chemistry *288*, 25025-25037.

Musumeci, G., Castorina, A., Magro, G., Cardile, V., Castorina, S., and Ribatti, D. (2015). Enhanced expression of CD31/platelet endothelial cell adhesion molecule 1 (PECAM1) correlates with hypoxia inducible factor-1 alpha (HIF-1α) in human glioblastoma multiforme. Experimental Cell Research *339*, 407-416.

Nishide, K., Nakatani, Y., Kiyonari, H., and Kondo, T. (2009). Glioblastoma formation from cell population depleted of Prominin1-expressing cells. PloS one *4*, e6869.

Nishiyama, A., Komitova, M., Suzuki, R., and Zhu, X. (2009). Polydendrocytes (NG2 cells): multifunctional cells with lineage plasticity. Nature reviews Neuroscience *10*, 9-22.

Norden, A.D., Drappatz, J., and Wen, P.Y. (2009). Antiangiogenic therapies for high-grade glioma. Nature reviews Neurology *5*, 610-620.

Noushmehr, H., Weisenberger, D.J., Diefes, K., Phillips, H.S., Pujara, K., Berman, B.P., Pan, F., Pelloski, C.E., Sulman, E.P., Bhat, K.P.*, et al.* (2010). Identification of a CpG Island Methylator Phenotype that Defines a Distinct Subgroup of Glioma. Cancer cell *17*, 510-522.

Nunes, M.C., Roy, N.S., Keyoung, H.M., Goodman, R.R., McKhann, G., 2nd, Jiang, L., Kang, J., Nedergaard, M., and Goldman, S.A. (2003). Identification and isolation of multipotential neural progenitor cells from the subcortical white matter of the adult human brain. Nature medicine *9*, 439-447.

Ogden, A.T., Waziri, A.E., Lochhead, R.A., Fusco, D., Lopez, K., Ellis, J.A., Kang, J., Assanah, M., McKhann, G.M., Sisti, M.B.*, et al.* (2008). Identification of A2B5+CD133-tumor-initiating cells in adult human gliomas. Neurosurgery *62*, 505-514; discussion 514-505.

Omuro, A., and DeAngelis, L.M. (2013). Glioblastoma and other malignant gliomas: A clinical review. JAMA *310*, 1842-1850.

Palmer, A.R., Jiang, D., and McAlpine, D. (2000a). Neural responses in the inferior colliculus to binaural masking level differences created by inverting the noise in one ear. Journal of neurophysiology *84*, 844-852.

Palmer, T.D., Willhoite, A.R., and Gage, F.H. (2000b). Vascular niche for adult hippocampal neurogenesis. Journal of Comparative Neurology *425*, 479-494.

Parkin, D.M., Bray, F., Ferlay, J., and Pisani, P. (2005). Global cancer statistics, 2002. Ca-Cancer J Clin *55*, 74-108.

Patel, A.P., Tirosh, I., Trombetta, J.J., Shalek, A.K., Gillespie, S.M., Wakimoto, H., Cahill, D.P., Nahed, B.V., Curry, W.T., Martuza, R.L.*, et al.* (2014). Single-cell RNA-seq highlights intratumoral heterogeneity in primary glioblastoma. Science *344*, 1396-1401.

Pedron, S. (2015). Effect of Hyaluronic Acid on Brain Cancer Development. Tissue Eng Pt A *21*, S177-S177.

Pedron, S., Becka, E., and Harley, B.A. (2013). Regulation of glioma cell phenotype in 3D matrices by hyaluronic acid. Biomaterials *34*, 7408-7417.

Pedron, S., Becka, E., and Harley, B.A. (2015). Spatially gradated hydrogel platform as a 3D engineered tumor microenvironment. Adv Mater *27*, 1567-1572.

Pedron, S., and Harley, B.A. (2013). Impact of the biophysical features of a 3D gelatin microenvironment on glioblastoma malignancy. J Biomed Mater Res A *101*, 3404-3415.

Pelloski, C.E., Mahajan, A., Maor, M., Chang, E.L., Woo, S., Gilbert, M., Colman, H., Yang, H., Ledoux, A., Blair, H.*, et al.* (2005). YKL-40 expression is associated with

poorer response to radiation end shorter overall survival in glioblastoma. Clinical Cancer Research *11*, 3326-3334.

Pen, A., Moreno, M.J., Martin, J., and Stanimirovic, D.B. (2007). Molecular markers of extracellular matrix remodeling in glioblastoma vessels: microarray study of laser-captured glioblastoma vessels. Glia *55*, 559-572.

Phillips, H.S., Kharbanda, S., Chen, R.H., Forrest, W.F., Soriano, R.H., Wu, T.D., Misra, A., Nigro, J.M., Colman, H., Soroceanu, L.*, et al.* (2006). Molecular subclasses of high-grade glioma predict prognosis, delineate a pattern of disease progression, and resemble stages in neurogenesis. Cancer cell *9*, 157-173.

Piao, Y., Liang, J., Holmes, L., Henry, V., Sulman, E., and de Groot, J.F. (2013). Acquired Resistance to Anti-VEGF Therapy in Glioblastoma Is Associated with a Mesenchymal Transition. Clinical Cancer Research *19*, 4392-4403.

Ramirez-Castillejo, C., Sanchez-Sanchez, F., Andreu-Agullo, C., Ferron, S.R., Aroca-Aguilar, J.D., Sanchez, P., Mira, H., Escribano, J., and Farinas, I. (2006). Pigment epithelium-derived factor is a niche signal for neural stem cell renewal. Nature neuroscience *9*, 331-339.

Rao, S.S. (2013). Glioblastoma behaviors in three-dimensional collagen-hyaluronan composite hydrogels. Acs Appl Mater Interfaces *5*, 9276-9284.

Reynolds, B.A., Tetzlaff, W., and Weiss, S. (1992). A multipotent EGF-responsive striatal embryonic progenitor cell produces neurons and astrocytes. The Journal of neuroscience : the official journal of the Society for Neuroscience *12*, 4565-4574.

Reynolds, B.A., and Weiss, S. (1992). Generation of neurons and astrocytes from isolated cells of the adult mammalian central nervous system. Science *255*, 1707-1710.

Ricci-Vitiani, L., Pallini, R., Biffoni, M., Todaro, M., Invernici, G., Cenci, T., Maira, G., Parati, E.A., Stassi, G., Larocca, L.M.*, et al.* (2010). Tumour vascularization via endothelial differentiation of glioblastoma stem-like cells. Nature *468*, 824-828.

Rich, J.N., and Eyler, C.E. (2008). Cancer stem cells in brain tumor biology. Cold Spring Harbor symposia on quantitative biology *73*, 411-420.

Saghatelyan, A. (2009). Role of blood vessels in the neuronal migration. Seminars in Cell & Developmental Biology *20*, 744-750.

Scholz, A., Harter, P.N., Cremer, S., Yalcin, B.H., Gurnik, S., Yamaji, M., Di Tacchio, M., Sommer, K., Baumgarten, P., Bahr, O.*, et al.* (2016). Endothelial cell-derived angiopoietin-2 is a therapeutic target in treatment-naive and bevacizumab-resistant glioblastoma. EMBO molecular medicine *8*, 39-57.

Schonberg, D.L., Lubelski, D., Miller, T.E., and Rich, J.N. (2013). Brain tumor stem cells: Molecular characteristics and their impact on therapy. Molecular aspects of medicine.

Schonberg, D.L., Lubelski, D., Miller, T.E., and Rich, J.N. (2014). Brain tumor stem cells: Molecular characteristics and their impact on therapy. Molecular aspects of medicine *39*, 82-101.

Seidlits, S.K., Khaing, Z.Z., Petersen, R.R., Nickels, J.D., Vanscoy, J.E., Shear, J.B., and Schmidt, C.E. (2010). The effects of hyaluronic acid hydrogels with tunable mechanical properties on neural progenitor cell differentiation. Biomaterials *31*, 3930-3940.

Sharma, A., and Shiras, A. (2016). Cancer stem cell-vascular endothelial cell interactions in glioblastoma. Biochemical and biophysical research communications *473*, 688-692.

Shen, Q., Goderie, S.K., Jin, L., Karanth, N., Sun, Y., Abramova, N., Vincent, P., Pumiglia, K., and Temple, S. (2004). Endothelial cells stimulate self-renewal and expand neurogenesis of neural stem cells. Science *304*, 1338-1340.

Shih, A.H., and Holland, E.C. (2006). Platelet-derived growth factor (PDGF) and glial tumorigenesis. Cancer letters *232*, 139-147.

Silva, J.M., Li, M.Z., Chang, K., Ge, W., Golding, M.C., Rickles, R.J., Siolas, D., Hu, G., Paddison, P.J., Schlabach, M.R.*, et al.* (2005). Second-generation shRNA libraries covering the mouse and human genomes. Nat Genet *37*, 1281-1288.

Sim, F.J., McClain, C.R., Schanz, S.J., Protack, T.L., Windrem, M.S., and Goldman, S.A. (2011). CD140a identifies a population of highly myelinogenic, migration-competent and efficiently engrafting human oligodendrocyte progenitor cells. Nature biotechnology *29*, 934-941.

Sim, F.J., Windrem, M.S., and Goldman, S.A. (2009). Fate determination of adult human glial progenitor cells. Neuron glia biology *5*, 45-55.

Singh, S.K., Clarke, I.D., Terasaki, M., Bonn, V.E., Hawkins, C., Squire, J., and Dirks, P.B. (2003). Identification of a cancer stem cell in human brain tumors. Cancer research *63*, 5821-5828.

Singh, S.K., Hawkins, C., Clarke, I.D., Squire, J.A., Bayani, J., Hide, T., Henkelman, R.M., Cusimano, M.D., and Dirks, P.B. (2004). Identification of human brain tumour initiating cells. Nature *432*, 396-401.

Smyth, G.K. (2005). limma: Linear Models for Microarray Data. In Bioinformatics and Computational Biology Solutions Using R and Bioconductor, R. Gentleman, V.J. Carey, W. Huber, R.A. Irizarry, and S. Dudoit, eds. (New York, NY: Springer New York), pp. 397-420.

Stiles, C.D., and Rowitch, D.H. (2008). Glioma stem cells: A midterm exam. Neuron *58*, 832-846.

Stratmann, A., Risau, W., and Plate, K.H. (1998). Cell type-specific expression of angiopoietin-1 and angiopoietin-2 suggests a role in glioblastoma angiogenesis. The American journal of pathology *153*, 1459-1466.

Stupp, R., Hegi, M.E., Mason, W.P., van den Bent, M.J., Taphoorn, M.J., Janzer, R.C., Ludwin, S.K., Allgeier, A., Fisher, B., Belanger, K.*, et al.* (2009). Effects of radiotherapy with concomitant and adjuvant temozolomide versus radiotherapy alone on survival in glioblastoma in a randomised phase III study: 5-year analysis of the EORTC-NCIC trial. The Lancet Oncology *10*, 459-466.

Stupp, R., Mason, W.P., van den Bent, M.J., Weller, M., Fisher, B., Taphoorn, M.J., Belanger, K., Brandes, A.A., Marosi, C., Bogdahn, U.*, et al.* (2005). Radiotherapy plus concomitant and adjuvant temozolomide for glioblastoma. The New England journal of medicine *352*, 987-996.

Sung, V., Stubbs, J.T., Fisher, L., Aaron, A.D., and Thompson, E.W. (1998). Bone sialoprotein supports breast cancer cell adhesion proliferation and migration through differential usage of the αvβ3 and αvβ5 integrins. Journal of Cellular Physiology *176*, 482-494.

Tchoghandjian, A., Baeza, N., Colin, C., Cayre, M., Metellus, P., Beclin, C., Ouafik, L.H., and Figarella-Branger, D. (2010). A2B5 Cells from Human Glioblastoma have Cancer Stem Cell Properties. Brain Pathology *20*, 211-221.

van den Bent, M.J., Dubbink, H.J., Marie, Y., Brandes, A.A., Taphoorn, M.J., Wesseling, P., Frenay, M., Tijssen, C.C., Lacombe, D., Idbaih, A.*, et al.* (2010). IDH1 and IDH2 mutations are prognostic but not predictive for outcome in anaplastic oligodendroglial tumors: a report of the European Organization for Research and Treatment of Cancer Brain Tumor Group. Clinical cancer research : an official journal of the American Association for Cancer Research *16*, 1597-1604.

van den Bent, M.J., Dubbink, H.J., Sanson, M., van der Lee-Haarloo, C.R., Hegi, M., Jeuken, J.W., Ibdaih, A., Brandes, A.A., Taphoorn, M.J., Frenay, M.*, et al.* (2009). MGMT promoter methylation is prognostic but not predictive for outcome to adjuvant PCV chemotherapy in anaplastic oligodendroglial tumors: a report from EORTC Brain Tumor Group Study 26951. Journal of clinical oncology : official journal of the American Society of Clinical Oncology *27*, 5881-5886.

van den Bent, M.J., Taphoorn, M.J., Brandes, A.A., Menten, J., Stupp, R., Frenay, M., Chinot, O., Kros, J.M., van der Rijt, C.C., Vecht Ch, J.*, et al.* (2003). Phase II study of first-line chemotherapy with temozolomide in recurrent oligodendroglial tumors: the European Organization for Research and Treatment of Cancer Brain Tumor Group Study 26971. Journal of clinical oncology : official journal of the American Society of Clinical Oncology *21*, 2525-2528.

Veeravagu, A., Bababeygy, S.R., Kalani, M.Y., Hou, L.C., and Tse, V. (2008). The cancer stem cell-vascular niche complex in brain tumor formation. Stem cells and development *17*, 859-867.

Verhaak, R.G., Hoadley, K.A., Purdom, E., Wang, V., Qi, Y., Wilkerson, M.D., Miller, C.R., Ding, L., Golub, T., Mesirov, J.P.*, et al.* (2010). Integrated genomic analysis identifies clinically relevant subtypes of glioblastoma characterized by abnormalities in PDGFRA, IDH1, EGFR, and NF1. Cancer cell *17*, 98-110.

Voronov, E., Shouval, D.S., Krelin, Y., Cagnano, E., Benharroch, D., Iwakura, Y., Dinarello, C.A., and Apte, R.N. (2003). IL-1 is required for tumor invasiveness and angiogenesis. Proceedings of the National Academy of Sciences of the United States of America *100*, 2645-2650.

Wang, C., Tong, X., and Yang, F. (2014). Bioengineered 3D brain tumor model to elucidate the effects of matrix stiffness on glioblastoma cell behavior using PEG-based hydrogels. Mol Pharm *11*, 2115-2125.

Wang, R., Chadalavada, K., Wilshire, J., Kowalik, U., Hovinga, K.E., Geber, A., Fligelman, B., Leversha, M., Brennan, C., and Tabar, V. (2010). Glioblastoma stem-like cells give rise to tumour endothelium. Nature *468*, 829-833.

Watkins, S., Robel, S., Kimbrough, I.F., Robert, S.M., Ellis-Davies, G., and Sontheimer, H. (2014). Disruption of astrocyte-vascular coupling and the blood-brain barrier by invading glioma cells. Nature communications *5*, 4196.

Watters, J.J., Schartner, J.M., and Badie, B. (2005). Microglia function in brain tumors. Journal of neuroscience research *81*, 447-455.

Wen, P.Y., and Kesari, S. (2008). Malignant gliomas in adults. The New England journal of medicine *359*, 492-507.

Wick, W., Weller, M., van den Bent, M., Sanson, M., Weiler, M., von Deimling, A., Plass, C., Hegi, M., Platten, M., and Reifenberger, G. (2014). MGMT testing--the challenges for biomarker-based glioma treatment. Nature reviews Neurology *10*, 372-385.

Xu, T., Qin, R., Zhou, J., Yan, Y., Lu, Y., Zhang, X., Fu, D., Lv, Z., Li, W., Xia, C.*, et al.* (2012). High bone sialoprotein (BSP) expression correlates with increased tumor grade and predicts a poorer prognosis of high-grade glioma patients. PloS one *7*, e48415.

Yan, H., Parsons, D.W., Jin, G., McLendon, R., Rasheed, B.A., Yuan, W., Kos, I., Batinic-Haberle, I., Jones, S., Riggins, G.J.*, et al.* (2009). IDH1 and IDH2 mutations in gliomas. The New England journal of medicine *360*, 765-773.

Zagzag, D., Amirnovin, R., Greco, M.A., Yee, H., Holash, J., Wiegand, S.J., Zabski, S., Yancopoulos, G.D., and Grumet, M. (2000). Vascular apoptosis and involution in

gliomas precede neovascularization: a novel concept for glioma growth and angiogenesis. Laboratory investigation; a journal of technical methods and pathology *80*, 837-849.

Zhong, J., Paul, A., Kellie, S.J., and O'Neill, G.M. (2010). Mesenchymal migration as a therapeutic target in glioblastoma. J Oncol *2010*, 430142.

Zhu, T.S., Costello, M.A., Talsma, C.E., Flack, C.G., Crowley, J.G., Hamm, L.L., He, X., Hervey-Jumper, S.L., Heth, J.A., Muraszko, K.M.*, et al.* (2011). Endothelial Cells Create a Stem Cell Niche in Glioblastoma by Providing NOTCH Ligands That Nurture Self-Renewal of Cancer Stem-Like Cells. Cancer research *71*, 6061-6072.

Zong, H., Verhaak, R.G.W., and Canoll, P. (2012). The cellular origin for malignant glioma and prospects for clinical advancements. Expert Review of Molecular Diagnostics *12*, 383-394.